

NVS-Adapter: Plug-and-Play Novel View Synthesis from a Single Image

Yoonwoo Jeong^{*†}
POSTECH

jeongyw12382@postech.ac.kr

Jinwoo Lee[†]
Kakao Brain

chopper.lee@kakaobrain.com

Chiheon Kim
Kakao Brain

chiheon.kim@kakaobrain.com

Minsu Cho[‡]
POSTECH

mscho@postech.ac.kr

Doyup Lee[‡]
Kakao Brain

doyup.lee@kakaobrain.com

Abstract

Transfer learning of large-scale Text-to-Image (T2I) models has recently shown impressive potential for Novel View Synthesis (NVS) of diverse objects from a single image. While previous methods typically train large models on multi-view datasets for NVS, fine-tuning the whole parameters of T2I models not only demands a high cost but also reduces the generalization capacity of T2I models in generating diverse images in a new domain. In this study, we propose an effective method, dubbed NVS-Adapter, which is a plug-and-play module for a T2I model, to synthesize novel multi-views of visual objects while fully exploiting the generalization capacity of T2I models. NVS-Adapter consists of two main components; view-consistency cross-attention learns the visual correspondences to align the local details of view features, and global semantic conditioning aligns the semantic structure of generated views with the reference view. Experimental results demonstrate that the NVS-Adapter can effectively synthesize geometrically consistent multi-views and also achieve high performance on benchmarks without full fine-tuning of T2I models. The code and data are publicly available in <https://postech-cvlab.github.io/nvsadapter/>.

1. Introduction

Novel View Synthesis (NVS) from a single image is an important task for a generative model to understand 3D geometry of visual objects and scenes. Given a single reference image of an object, the goal is to synthesize multiple images under novel viewpoints that are consistent with the reference image. Compared to the conventional setting [36, 39] with hundreds of reference views, this challenging problem

^{*}Work done during an internship at Kakao Brain

[†]Equal Contribution

[‡]Corresponding author



Figure 1. Our NVS-Adapter is capable of generating novel views from a reference image while preserving the generation capacity of the pretrained text-to-image model.

with a single reference view inevitably suffers from the limited information in generating unseen and occluded regions. Generative models are thus necessitated to learn effective priors for geometric and semantic understanding of various objects and scenes in the real world.

Recent advanced generative models have made remarkable progress in reconstructing 3D geometry from a single image. For example, diffusion models [20, 25, 57] generate impressive multi-views [64, 72] or neural fields [2, 5, 17] by learning from multi-view datasets [6, 10, 47, 68]. Since these methods require categorical priors of predefined 3D objects due to the limited scale of 3D datasets, compared with image datasets [3, 50], more recent methods [31–34, 54, 55] attempt to transfer a Text-to-Image (T2I) model [48]

on Objaverse [9, 10] by fine-tuning it over one billion parameters of the T2I models. However, the process of fine-tuning the original attention modules of T2I models may lead to a catastrophic forgetting and deteriorate the generalization capacity for generating diverse images [32, 55].

In this study, we introduce an effective transfer-learning framework with *NVS-Adapter* to synthesize novel views of diverse objects from a single image while fully exploiting the generalization capacity of T2I models. Inspired by seminal studies of controllable image generation [29, 37, 71], we propose to learn a plug-and-play adaptation module into T2I models to align the semantic and geometry of novel multi-views without extensive finetuning of T2I models. The proposed NVS-Adapter consists of two main components: *view-consistency cross-attention* and *global semantic conditioning*. The view-consistency cross-attention learns visual correspondences between views to align their local details, while efficiently aggregating the features of multi-views to be generated. The global semantic conditioning exploits the reference view to align the semantic features of generated multi-views. Our experiments demonstrate that a T2I model with our NVS-Adapter synthesizes geometrically consistent multi-views, achieving competitive performance with previous approaches as shown in Figure 1.

Our main contributions can be summarized as follows: 1) We propose a novel plug-and-play NVS-Adapter with view-consistency cross-attention and global semantic conditioning for T2I models to synthesize novel views of diverse objects. 2) Our view-consistency cross-attention can effectively align the local details of different views to provide geometrically consistent multi-views. 3) The experiments demonstrate the efficacy of our NVS-Adapter to exploit the generalization capacity of T2I models for NVS and 3D reconstruction.

2. Related Work

Generative Models for 3D Objects Generative models have shown remarkable progress in synthesizing 3D objects. Geometry-aware generative models [4, 16, 42, 65] adopt adversarial training to implicitly learn 3D representation of faces [4] and scenes [42, 65] from 2D images. Recent studies train diffusion models [20, 25, 57] to directly generate 3D representations [2, 8, 14, 23, 24, 38, 40, 41, 43, 56, 69]. Diffusion models are also trained on multi-view datasets [6, 47, 68] to synthesize novel views via cross-attentions [64, 72] or implicit feature fields [5, 17, 67].

Text-to-3D Generation via 2D Diffusion Prior Given a text prompt, a text-to-image (T2I) diffusion model can generate a 3D representation without 3D data. The seminal work [44] proposes a score distillation sampling (SDS) to update the 3D representation, whose rendered images are supervised by the scores of T2I models. Along with the

advances in neural fields [39, 52, 61, 62], the existing studies [7, 30, 60, 63] have consistently improved the performance of SDS. In addition, low-rank adaptation [21], structural conditions [71], and view-dependent texts [44] are exploited to maintain the multi-view consistency of generated 3D representations [35, 51, 63]. However, the geometric consistency of generated 3D contents is unsatisfactory despite their high-fidelity, since the training data of T2I models does not contain precise information of 3D geometry.

Finetuning T2I Models for Novel View Synthesis Existing studies modify and finetune T2I models on multi-view datasets to generate high-quality and diverse images for novel view synthesis. Zero-1-to-3 [9, 32] concatenates a reference image into the input of U-Net after modifying text cross-attentions for image embeddings with relative camera extrinsics [27]. Despite finetuning on Objaverse [9, 10], generated views suffer from geometric inconsistency and inaccurate camera view points, since the model cannot explicitly learn visual correspondences between the reference and generated views [54]. MVDream [55], ConsistNet [66], and SyncDreamer [33] build on Zero-1-to-3 to synthesize multiple novel views, employing 3D self-attentions [55] and unprojection [33, 66]. Wonder3D [34] finetunes the Stable Diffusion Image Variations Model [27] to generate multi-view normal maps alongside color images. The concurrent works, Zero123++ [54] and One-2-3-45++ [31], adopt the reference attention technique [70] and finetune the original self-attentions for NVS from a single image.

3. Methods

We propose an effective framework with NVS-Adapter in Figure 2 to synthesize novel views from a single reference view of diverse 3D objects, while preserving the original capability of T2I models. After we first introduce the preliminaries of diffusion models and novel view synthesis, we explain the formulation of diffusion models for novel view synthesis. Then, we present the details of our NVS-Adapter for synthesizing geometrically consistent multi-views of visual objects in a plug-and-play manner.

3.1. Preliminaries

Diffusion Models Diffusion models learn a data distribution $q(\mathbf{x})$ using gradually corrupted latent variables $\mathbf{x}_1, \dots, \mathbf{x}_T$, where $q(\mathbf{x}_t|\mathbf{x}_0) := \mathcal{N}(\mathbf{x}_t; \sqrt{\alpha_t}\mathbf{x}_0, (1 - \alpha_t)\mathbf{I})$ and $\mathbf{x}_0 = \mathbf{x}$. Then, a diffusion model $p_\theta(\mathbf{x}_{0:T})$ aims to predict the reverse process of the Markov chain with Gaussian transitions to denoise the latents as $p_\theta(\mathbf{x}_{0:T}) := p(\mathbf{x}_T) \prod_{t=1}^T p_\theta(\mathbf{x}_{t-1}|\mathbf{x}_t)$, where $p(\mathbf{x}_T) := \mathcal{N}(\mathbf{x}_T|\mathbf{0}, \mathbf{I})$, $p_\theta(\mathbf{x}_{t-1}|\mathbf{x}_t) := \mathcal{N}(\mathbf{x}_t; \mu_\theta(\mathbf{x}_t, t), \sigma_t^2\mathbf{I})$, and σ_t is a constant at t . Given a constant α_t at timestep t , the predicted mean is defined as $\mu_\theta(\mathbf{x}_t, t) := (\mathbf{x}_t - \sqrt{1 - \alpha_t}\epsilon_\theta(\mathbf{x}_t, t))/\sqrt{\alpha_t}$, and

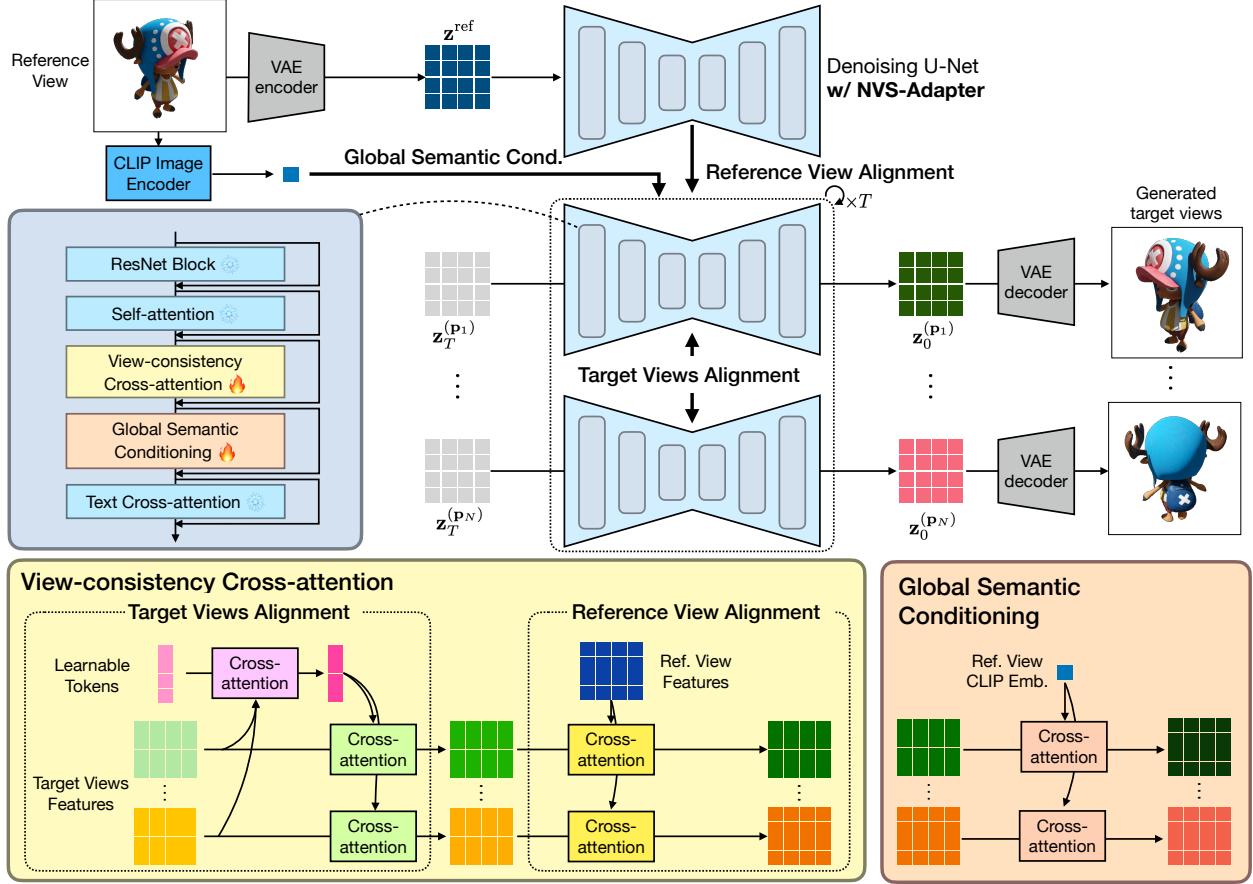


Figure 2. Overview of our framework. NVS-Adapter synthesizes novel views by incorporating two components into each U-Net block of a pretrained T2I model: *view-consistency cross-attention* which aligns features of each target view with the relevant features of other views, and *global semantic conditioning* which aligns the features of target views with the global semantic structure of the reference.

the noise predictor ϵ_θ is trained to minimize the reweighted variational lower bound [20]:

$$L_{\text{simple}} = \mathbb{E}_{t, \mathbf{x}_0, \epsilon} [\|\epsilon - \epsilon_\theta(\mathbf{x}_t, t)\|^2], \quad (1)$$

where $\mathbf{x}_t = \sqrt{\alpha_t} \mathbf{x}_0 + \sqrt{1 - \alpha_t} \epsilon$, and $\epsilon \sim \mathcal{N}(\mathbf{0}, \mathbf{I})$.

Latent Diffusion Models The two-stage framework of latent diffusion models (LDMs) [48] can effectively generate high-resolution images. In the first stage, an auto-encoder [15], which consists of an encoder \mathcal{E} and a decoder \mathcal{D} , learns to compress a high-resolution RGB image $\mathbf{x} \in \mathbb{R}^{H \times W \times 3}$ into a low-resolution feature map $\mathbf{z} = \mathcal{E}(\mathbf{x}) \in \mathbb{R}^{H/f \times W/f \times C}$, and the decoder reconstructs the image from the latent as $\mathbf{x} \approx \mathcal{D}(\mathcal{E}(\mathbf{x}))$, where f is a downsampling factor and C is the dimensionality of latents. Then, the U-Net [11, 49] of the diffusion process is processed on the latent space of \mathbf{z} instead of \mathbf{x} . Each U-Net block of T2I models, such as Stable Diffusion, comprises a ResNet block followed by a self-attention block of image features and a cross-attention between image and text features.

Novel View Synthesis from a Single Image Given a reference view of a 3D object, we aim to generate its rendered images from novel viewpoints. Let the reference RGB image $\mathbf{x}^{\text{ref}} \in \mathbb{R}^{H \times W \times 3}$, N relative camera viewpoints to a reference viewpoint $\mathbf{P} = \{\mathbf{p}_1, \dots, \mathbf{p}_N\}$, the rendered novel views $\mathbf{x}^{(\mathbf{P})} = \{\mathbf{x}^{(\mathbf{p}_1)}, \dots, \mathbf{x}^{(\mathbf{p}_N)}\}$ be given, where $\mathbf{p}_i = [R_i; T_i] \in \mathbb{R}^{3 \times 4}$ is i -th camera viewpoint with relative camera rotation $R_i \in \mathbb{R}^{3 \times 3}$ and translation $T_i \in \mathbb{R}^3$, and its rendered novel view $\mathbf{x}^{(\mathbf{p}_i)}$, respectively. Then, a generative model learns a conditional distribution $q(\mathbf{x}^{(\mathbf{P})} | \mathbf{x}^{\text{ref}}, \mathbf{P})$ to synthesize novel views $\mathbf{x}^{(\mathbf{P})}$ of a reference view \mathbf{x}^{ref} . For the brevity of notation, we denote $q(\mathbf{x}^{(\mathbf{P})} | \mathbf{x}^{\text{ref}}, \mathbf{P})$ by $q(\mathbf{x}^{(\mathbf{P})} | \mathbf{x}^{\text{ref}})$. Note that a powerful generative model such as a diffusion model is required, since the model has to extrapolate unseen or occluded parts of the 3D object.

3.2. LDMs for NVS from a Single Image

We formulate LDMs for NVS from a single reference image, since we aim to adapt the pretrained LDM, Stable Diffusion, for NVS. A LDM learns a conditional distribution $q(\mathbf{z}^{(\mathbf{P})} | \mathbf{z}^{\text{ref}})$, where the latents of a reference view $\mathbf{z}^{\text{ref}} =$

$\mathcal{E}(\mathbf{x}^{\text{ref}})$ and the latents of target views $\mathbf{z}^{(\mathbf{P})} = \{\mathbf{z}^{(\mathbf{P}_i)} = \mathcal{E}(\mathbf{x}^{(\mathbf{P}_i)})\}_{i=1}^N$. Here, the approximate posterior is defined as $q(\mathbf{z}_t^{(\mathbf{P})} | \mathbf{z}_0^{(\mathbf{P})}, \mathbf{z}^{\text{ref}}) = \prod_{i=1}^N q(\mathbf{z}_t^{(\mathbf{P}_i)} | \mathbf{z}_0^{(\mathbf{P}_i)})$, where the noised latents of target views are $\mathbf{z}_t^{(\mathbf{P}_i)} = \sqrt{\alpha_t} \mathbf{z}_0^{(\mathbf{P}_i)} + \sqrt{1 - \alpha_t} \epsilon$, and $\epsilon \sim \mathcal{N}(\mathbf{0}, \mathbf{I})$. The diffusion model $p_\theta(\mathbf{z}_{t-1}^{(\mathbf{P})} | \mathbf{z}_t^{(\mathbf{P})}, \mathbf{z}^{\text{ref}})$ learns to denoise the noised latents of N target views at a timestep t to synthesize consistent multi-views. Meanwhile, note that previous approaches [32, 64] assume that the novel views $\mathbf{z}^{(\mathbf{P})}$ are independently generated as $p_\theta(\mathbf{z}_{t-1}^{(\mathbf{P})} | \mathbf{z}_t^{(\mathbf{P})}, \mathbf{z}^{\text{ref}}) = \prod_{i=1}^N p_\theta(\mathbf{z}_{t-1}^{(\mathbf{P}_i)} | \mathbf{z}_t^{(\mathbf{P}_i)}, \mathbf{z}^{\text{ref}})$ for a simple modeling. However, the assumption can lead to the geometrically inconsistent results, since the generating process cannot align the details and geometry between target views. Thus, our denoising process aligns the views to consider their correspondences:

$$p_\theta(\mathbf{z}_{t-1}^{(\mathbf{P})} | \mathbf{z}_t^{(\mathbf{P})}, \mathbf{z}^{\text{ref}}) = \prod_{i=1}^N p_\theta(\mathbf{z}_{t-1}^{(\mathbf{P}_i)} | \mathbf{z}_t^{(\mathbf{P}_i)}, \mathbf{z}^{\text{ref}}), \quad (2)$$

while each target view is also aligned with the reference \mathbf{z}^{ref} . To preserve the fine-grained details of visual objects at every denoising step, we do not corrupt latent features from a reference view.

3.3. NVS-Adapter

In this section, we explain the details of *NVS-Adapter* to adapt a T2I model for synthesizing consistent novel multi-views from a single reference image. As part of our training approach, where we maintain the parameters of the T2I model, we incorporate NVS-Adapter into the middle of each U-Net block as illustrated in Figure 2. The model processes features of each view separately and effectively align view features using two components of a *view-consistency cross-attention* and *global semantic conditioning*. The view-consistency cross-attention enables the intermediate features of a target view to aggregate the matched features of the other target views and the reference view. Then, we use the global semantic conditioning to align the features of target views with the global semantic structure of the reference image.

3.3.1 View-Consistency Cross-Attention

Our view-consistency cross-attention sequentially conduct the *target views alignment* and *reference view alignment* with target views and a reference view, respectively. Since they are applied to the same operations at every block, we describe the operations in one U-Net block without the loss of generality.

Target Views Alignment Let a pretrained T2I model separately extract the features of target views $\mathbf{f}^{(\mathbf{P})} =$

$\{\mathbf{f}^{(\mathbf{P}_i)}\}_{i=1}^N$ with a ResNet and a self-attention block, where $\mathbf{f}^{(\mathbf{P}_i)} \in \mathbb{R}^{h \times w \times c}$ is the features of i -th target view with $h \times w$ resolution and c channels. We aggregate the features of the target views using L learnable tokens $\mathbf{q} \in \mathbb{R}^{L \times c}$ as

$$\bar{\mathbf{q}} := \text{MHA}(\mathbf{Q} = \mathbf{q}, \mathbf{KV} = \mathbf{f}^{(\mathbf{P})} + \mathbf{v}^{(\mathbf{P})}), \quad (3)$$

where \mathbf{Q} and \mathbf{KV} denote query and key-value of a multi-head attention (MHA) [59] operation, and $\mathbf{v}^{(\mathbf{P})} = \{\mathbf{v}^{(\mathbf{P}_i)}\}_{i=1}^N$ includes the positional embeddings for N feature maps on relative camera poses \mathbf{P} . When we encode $\mathbf{v}^{(\mathbf{P}_i)} \in \mathbb{R}^{h \times w \times c}$ under i -th camera relative into sinusoidal embeddings [36], we represent each ray position on the Plücker coordinate [12] to effectively learn a geometric relation between rays. We remark that the parameters of learnable tokens \mathbf{q} are shared across all target views. Subsequently, each target view leverages $\bar{\mathbf{q}}$ to aggregate the matched features from other target views as

$$\mathbf{f}_{\text{TA}}^{(\mathbf{P})} := \mathbf{f}^{(\mathbf{P})} + \text{MHA}(\mathbf{Q} = \mathbf{f}^{(\mathbf{P})} + \mathbf{v}^{(\mathbf{P})}, \mathbf{KV} = \bar{\mathbf{q}}), \quad (4)$$

where $\mathbf{f}_{\text{TA}}^{(\mathbf{P})}$ is target-views-aligned feature maps of $\mathbf{f}^{(\mathbf{P})}$.

Reference View Alignment We further perform reference view alignment to ensure the geometric consistency of details in the generated target views with the reference view, which is the only condition for NVS from a single image. After the target views alignment in Eq. (4), we further conduct an additional MHA operation as

$$\mathbf{f}_{\text{RA}}^{(\mathbf{P})} := \mathbf{f}_{\text{TA}}^{(\mathbf{P})} + \text{MHA}(\mathbf{Q} = \mathbf{f}_{\text{TA}}^{(\mathbf{P})} + \mathbf{v}^{(\mathbf{P})}, \mathbf{KV} = \mathbf{f}^{\text{ref}} + \mathbf{v}^{\text{ref}}), \quad (5)$$

where \mathbf{f}^{ref} is the ResNet features of the reference view, and \mathbf{v}^{ref} is its positional embeddings. The reference view alignment is also applied to the reference features, considering it as a self-attention:

$$\mathbf{f}_{\text{RA}}^{\text{ref}} := \mathbf{f}^{\text{ref}} + \text{MHA}(\mathbf{Q} = \mathbf{f}_{\text{TA}}^{\text{ref}} + \mathbf{v}^{\text{ref}}, \mathbf{KV} = \mathbf{f}^{\text{ref}}). \quad (6)$$

The aligned features $\mathbf{f}_{\text{RA}}^{(\mathbf{P})}$ and $\mathbf{f}_{\text{RA}}^{\text{ref}}$ become the input of the cross-attention, which conditions the features on text inputs of T2I models, while processing each view. Although our NVS task does not require texts, we remain the cross-attention of texts to preserve the original T2I models.

Note that our target views alignment employs the latent bottleneck $\bar{\mathbf{q}}$ in Eq. (3), similar to Perceiver [22], for an efficient alignment of target views. Although simply using a self-attention across the features of all target views is available, its computational cost has quadratic complexity as $O(N^2 h^2 w^2)$ for $\mathbf{f}^{(\mathbf{P})}$. However, our method requires $O(LNhw)$ and efficiently aggregates the features of target views to synthesize consistent multi-views at once.

Table 1. Comparison of novel view synthesis scores on Objaverse [10] with Zero-1-to-3 [32] and Zero123-XL [9].

	PSNR(\uparrow)	SSIM(\uparrow)	LPIPS(\downarrow)
Zero-1-to-3	19.52	0.8603	0.1251
Zero123-XL	17.71	0.8258	0.1552
ours	19.58	0.8658	0.1135

Table 2. NVS performance on Google Scanned Objects [13].

	PSNR	SSIM	LPIPS
Zero-1-to-3	18.36 \pm 0.02	0.8418 \pm 0.0005	0.1283 \pm 0.0006
Zero123-XL	18.46 \pm 0.11	0.8351 \pm 0.0015	0.1267 \pm 0.0009
ours	18.80 \pm 0.07	0.8469 \pm 0.0010	0.1207 \pm 0.0010

Table 3. The effects of the number of learnable tokens $L = h \times w \times c$ in target views alignment on NVS of the GSO dataset.

	PSNR	SSIM	LPIPS
$c = 0.5$	18.26 \pm 0.05	0.8406 \pm 0.0010	0.1277 \pm 0.0007
$c = 1$	18.56 \pm 0.09	0.8446 \pm 0.0018	0.1243 \pm 0.0015
$c = 2$	18.51 \pm 0.10	0.8441 \pm 0.0015	0.1251 \pm 0.0008

3.3.2 Global Semantic Conditioning

Our global semantic conditioning incorporates a cross-attention to align the features of all the views with the global semantics of a visual object. Note that the task of NVS assumes that a reference is given without its text captions, compared with T2I that leverages the text inputs as the global conditions. We extract the CLIP [45] image embedding of the reference view to conduct a cross-attention between the features of each view and the CLIP image embedding as shown in Figure 2. Although reusing the text cross-attention [53] is viable, we train addition cross-attention for global semantic conditioning to achieve high performance. Since we preserve the cross-attention for texts, our framework can also synthesize multi-views from a text prompt after generating a reference image from the text.

4. Experiments

In this section, we conduct extensive experiments to demonstrate the effectiveness of our NVS-Adapter. After we evaluate our framework on NVS benchmarks, we show the results of 3D generation such as image-to-3D and text-to-3D. We also conduct in-depth study to analyze the efficacy of our NVS-Adapter to understand the geometry over different viewpoints of visual objects.

We implement our NVS-Adapter on Stable Diffusion 2.1-base [1] and train our framework on Objaverse [10], which includes 800K 3D assets. We adopt the same training data of rendered views with 256 resolution as Zero-1-to-3 [32] for a fair comparison. Our NVS-Adapter uses $h \times w$

learnable tokens \mathbf{q} for target views alignment in Eq. (3) at every U-Net block, while aggregating $N = 4$ target views. Our model is trained for 200K iterations with 256 batch size, using 16 NVIDIA A100 80GB GPUs for 5 days. We attach the implementation details to Appendix.

4.1. Novel View Synthesis from a Single Image

We evaluate our framework on the validation split of Objaverse [10] and a subset of Google Scanned Objects (GSO) containing high-quality scanned 3D assets. We use the 12 rendered views of 3D assets provided by Zero-1-to-3 and select the first image as a reference view. Since we randomly select N target views among 12 views, we report the mean and standard deviation of results with three repetitions. Table 1 shows the competitive results with previous methods of Zero-1-to-3 and Zero123-XL in terms of PSNR, SSIM, and LPIPS [58]. In Table 2, our NVS-Adapter also outperforms Zero-1-to-3 and Zero123-XL on GSO, achieving high generalization performance. We remark that Zero-1-to-3 and Zero123-XL finetune over one billion parameters, and Zero123-XL learns 12 times more 3D assets than our NVS-Adapter. Thus, our plug-and-play NVS-Adapter can effectively adapt a T2I model to synthesize novel views from a single image.

Figure 3 visualizes the synthesized novel views to compare our NVS-Adapter with previous methods. Zero-1-to-3, Zero123-XL, and NVS-Adapter($N=1$) commonly suffer from the inconsistency of generated views, since they cannot synthesize multi-views at once. However, the NVS-Adapter ($N=1$) shows better correspondences between the reference and target views than Zero-1-to-3, since the view-consistency cross-attention learn the correspondences between view features. In addition, our NVS-Adapter ($N=4$) can align the features of multi-views and effectively generate geometrically consistent multi-views at once.

4.2. 3D Reconstruction

We leverage our framework with NVS-Adapter to reconstruct 3D geometry from a single image, incorporating Score Distillation Sampling (SDS) [44]. We freeze the parameters of our framework and optimize an Instant-NGP [39] to generate 3D consistent representations. We use the threestudio [18] implementations based on the setting of Zero-1-to-3 to compare our framework with other methods. We also employ opacity regularization to reduce noisy structures. In the coarse stage of training, we optimize the model for 5,000 iterations with batch size 16. Following the coarse stage, we further optimize the model for 3,000 iterations with a reduced batch size of 8. We sample a timestep t in the range [0.02, 0.98] and linearly decay the maximum timestep t_{max} to 0.5 during coarse stage [30].

Figure 4 compares the generated 3D representations via SDS of Zero-1-to-3, Zero123-XL, and our framework with

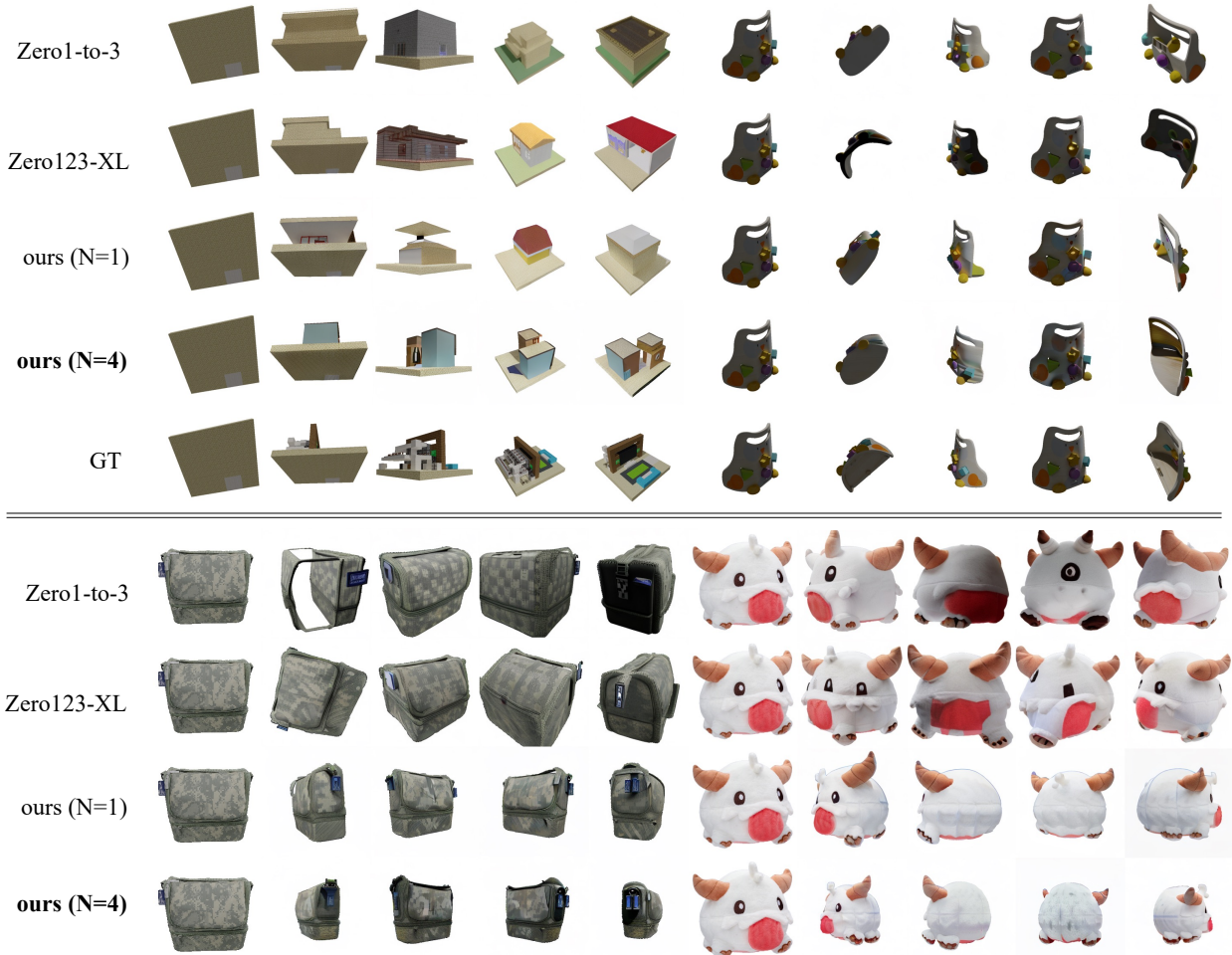


Figure 3. Novel view synthesis examples by Zero-1-to-3, Zero123-XL, and our NVS-Adapter with $N = 1$ and $N = 4$. Top images: NVS results conditioned on an image from Objaverse and GSO validation set. Bottom images: NVS results conditioned on a single image used in SyncDreamer [33]. The first column presents a reference image, and the rest of four columns are synthesized views by each model.

NVS-Adapter. We first generate images from the input texts as the reference views to compare our framework with Dreamfusion [44]. Compared with the oversimplified results of Dreamfusion, Zero-1-to-3, Zero123-XL, and our framework can generate 3D following the high fidelity of images generated from texts. However, Zero-1-to-3 and Zero123-XL suffer from geometric inconsistency, but our framework shows high-quality results following the reference images. Our framework also shows competitive results of image-to-3D, while generating geometrically consistent 3D representations compared with other methods.

4.3. Ablation Study

We conduct an extensive ablation study to evaluate the efficacy of our NVS-Adapter in synthesizing novel views. Due to the computational costs, we evaluate the trained models after 100K training iterations for the ablation study.

Table 4. The effects of the number of target views N on GSO.

	PSNR	SSIM	LPIPS
$N = 1$	18.45 ± 0.05	0.8409 ± 0.0003	0.1240 ± 0.0004
$N = 2$	18.70 ± 0.05	0.8453 ± 0.0010	0.1215 ± 0.0007
$N = 4$	18.56 ± 0.09	0.8446 ± 0.0018	0.1243 ± 0.0015
$N = 6$	17.85 ± 0.04	0.8333 ± 0.0017	0.1335 ± 0.0013

Table 5. Ablation study on a global semantic conditioning (GSC) in a view-consistency cross-attention for NVS of the GSO dataset.

	PSNR	SSIM	LPIPS
ours	18.45 ± 0.05	0.8409 ± 0.0003	0.1240 ± 0.0002
w/o GSC	18.27 ± 0.05	0.8388 ± 0.0007	0.1254 ± 0.0004

The number of learnable tokens. We evaluate the effects of learnable tokens q to aggregate the features of tar-

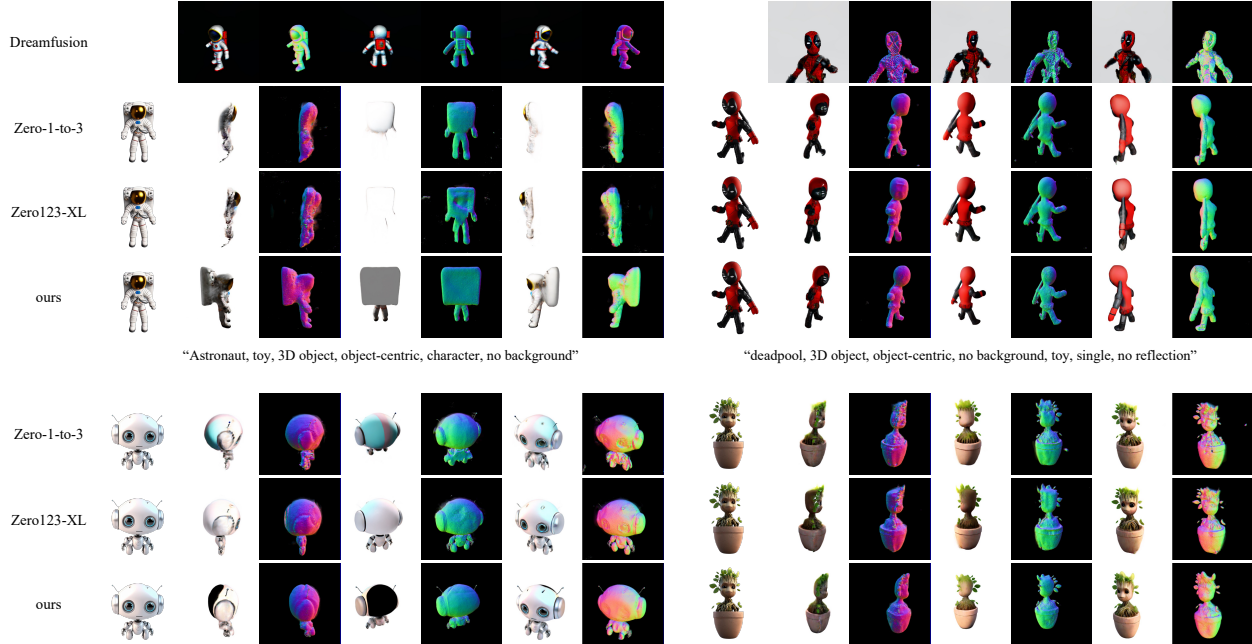


Figure 4. 3D reconstruction examples via Score Distillation Sampling (SDS) with baselines and our NVS-Adapter. Top images shows 3D reconstructions results conditioned on an image generated by T2I model, and bottom images shows results on an image in the wild.

Table 6. The effects of ray positional embeddings in the view-consistency cross-attention on NVS of the GSO dataset.

	PSNR	SSIM	LPIPS
extrinsic	18.02 ± 0.02	0.8329 ± 0.0006	0.1298 ± 0.000
ray o, ray d	18.41 ± 0.03	0.8423 ± 0.0004	0.1254 ± 0.0004
Plücker	18.45 ± 0.05	0.8409 ± 0.0003	0.1240 ± 0.0002

Table 7. The performance improvements of NVS-Adapter after finetuning the whole parameters.

	PSNR	SSIM	LPIPS
Zero-1-to-3	18.34	0.8424	0.1283
ours	18.87 ± 0.02	0.8477 ± 0.0000	0.1185 ± 0.0001
w/ full-tuning	19.00 ± 0.05	0.8488 ± 0.0007	0.1151 ± 0.0006

get views in Eq. (3). With a fixed number of target views $N = 4$, we vary the number of learnable tokens $L = h \cdot w \cdot c$ with $c = 0.5, 1, 2$ for a $h \times w$ resolution U-Net block. Table 3 shows that increasing the learnable tokens improves the results, since a large number of tokens can easily preserve the information of target views. However, NVS-Adapter with $N = 4$ achieves the best performance with $L = h \times w$ having fewer tokens than $N \times h \times w$. Thus, our target views alignment is effective to aggregate the features of target views into a fixed number of tokens instead of exploiting a vanilla cross-attention.

The number of target views. We analyze the effects of the number of target views N , since our NVS-Adapter can generate N target views at once. NVS-Adapters with $N = 1, 2, 4$ demonstrate comparable performance, but expanding to $N = 6$ deteriorates the overall performance, since the capacity of $L = h \times w$ learnable tokens is limited to aggregate $N > 4$ target views. Although NVS-Adapter with $N = 2$ achieves the best quantitative results, we choose $N = 4$ for the capability to consistently synthesize multi-views in a single generation as shown in Figure 3.

Effects of global semantic conditioning. We conduct an ablation study to validate the effectiveness of global semantic conditioning. Table 5 shows that leveraging the CLIP image features of a reference view enhances the semantic consistency of synthesized target views. In the Appendix, the novel views generated without global semantic conditioning suffer from lower quality due to the lack of semantic understanding of visual objects.

Ray positional embeddings. We examine the effects of ray positional embeddings on the view-consistency cross-attention. We change Plücker coordinates, which represent the ray positions in view features, into the offset and direction vectors of rays. In addition, we also compare the results using the embedding of camera extrinsic parameters, which is applied in Zero-1-to-3, instead of rays. Table 6 shows that utilizing each ray’s position improves the performance, since it allows our view-consistency cross-attention to lever-

Table 8. NVS performance of NVS-Adapter with depth-conditioned ControlNet on the validation set of Objaverse.

	PSNR	SSIM	LPIPS
w/ depth	20.53	0.8872	0.0900
w/o depth	17.71	0.8512	0.1303

age ray geometry for matching view correspondences.

The effects of full finetuning. In Table 7, we evaluate the performance of our framework after training all parameters, including the T2I model, for 200K iterations. Full finetuning of the model outperforms our plug-and-play approach, since full finetuning updates over one billion parameters tailored to NVS. However, our framework shows competitive results compared to the fully finetuned model, while preserving the original capability of T2I models. These results emphasize the effectiveness of our plug-and-play NVS-Adapter in enabling a T2I model to generate multi-views from images or texts, along with T2I generation.

4.4. Visualization Analysis of Cross-Attention Maps

We analyze the role of our view-consistency cross-attention to align the features of target and reference views. We visualize the mean of cross-attention maps in the last U-Net block at timestep $t = 800$ over the attention heads.

Target views alignment. Figure 5 visualizes the cross-attention maps that use learnable tokens as queries and the target views as keys. Each learnable token effectively aggregates and encodes the information of target views based on the semantic and positional features, reducing redundancy. For example, token 1 aggregates the white background of all target views, and token 2 attends to prominent regions in the foreground. Meanwhile, token 3 attends to a specific region of the foreground, while aggregating the same positions across different viewpoints. Thus, our method aggregates the features of target view features into a fixed number of tokens, enabling efficient synthesis of well-aligned multi-views.

Reference view alignment. Figure 6 visualizes the cross-attention maps, considering a target and reference view as a query and a key, respectively. Note that the highlighted regions in attention maps are corresponding to the query regions (red box) in Figure 6. That is, our reference view alignment focuses on matching target and reference view correspondences, aggregating the local details from the reference view for consistent synthesis.

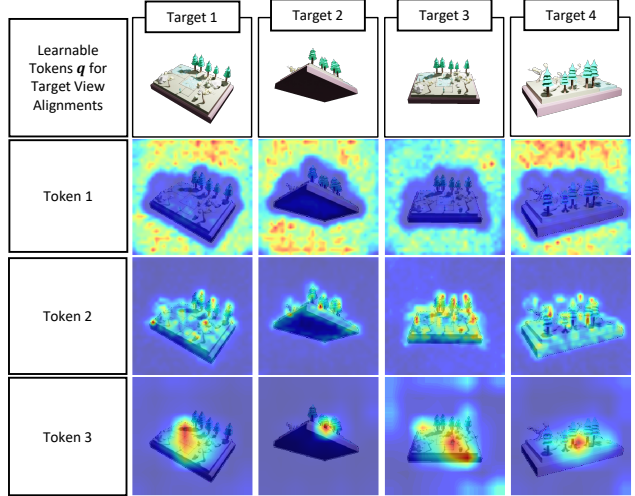


Figure 5. Visualization of attention maps of target views alignment. Each token aggregates different regions of target views.

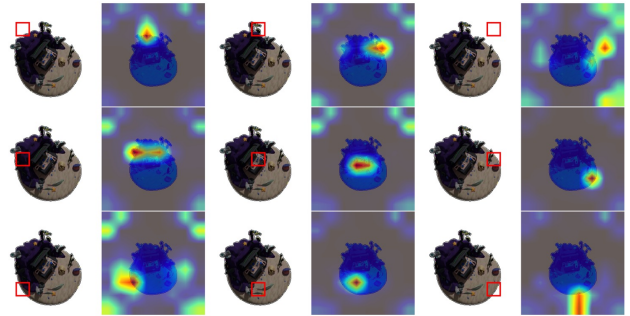


Figure 6. Visualization of attention maps of reference view alignment. The queries in the target view (red boxes, left) correspond to the highlighted regions in the reference view (right).

4.5. Compatibility with ControlNets

Since we preserve the original parameters of T2I models, our framework with NVS-Adapter is compatible with other plug-and-play modules such as ControlNets [71]. After we additionally train our NVS-Adapter on Stable Diffusion v1.5 [48], we combine the trained NVS-Adapter with the depth-conditioned ControlNet. Specifically, we use DPT-hybrid network [46] to extract a mono-depth map of each novel view of a given 3D asset as depth conditions of novel views. We use the validation set of Objaverse [10] to evaluate the compatibility of our NVS-Adapter with ControlNets. Table 8 shows that our NVS-Adapter can exploit the depth conditions to significantly improve NVS performance. Figure 7 also shows that the synthesized novel views follow the geometry of depth conditions, while validating that our NVS-Adapter is fully compatible with other plug-and-play modules of T2I models. Note that our framework does not require additional training for the compatibility with ControlNets, different from previous approaches [54].

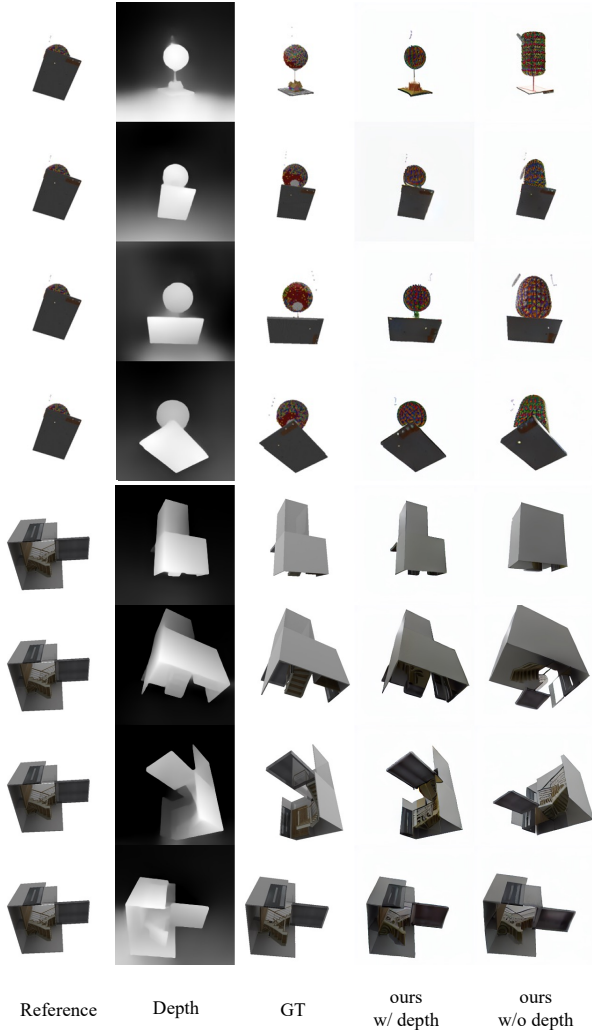


Figure 7. Examples of novel view synthesis using our NVS-Adapter with and without depth conditions.

5. Conclusion

We have proposed an effective transfer-learning framework with a plug-and-play NVS-Adapter for T2I models to synthesize geometrically consistent multi-views from a single image. Our NVS-Adapter employs view-consistency cross-attention for aligning target and reference views, and the embedding of a reference view is used for the global semantic condition of views. The experimental results show that our framework with the NVS-Adapter achieves high performance in NVS and 3D reconstruction tasks without finetuning T2I models. In addition, we have conducted an in-depth analysis to validate how our NVS-Adapter efficiently aggregates the information of target views and aligns the details of multi-views using cross-attentions.

Although our framework can synthesize consistent multi-views of diverse objects, we have generated a 3D

representation of visual objects via SDS of a large diffusion model. We expect that increasing the number of target views enables a neural field to be directly optimized via the generated multi-views, reducing the generation time of neural fields. Exploiting generalizable neural fields [26, 28, 31], which can infer 3D representations from multi-views, is worth exploration to circumvent the need for explicit optimization of neural fields per each sample. Furthermore, generating novel views of natural scenes from a single image is an interesting future work, expanding beyond visual objects.

References

- [1] Stability AI. Stable diffusion version 2. <https://github.com/Stability-AI/stablediffusion>, 2022. 5, 13
- [2] Titas Anciukevičius, Zexiang Xu, Matthew Fisher, Paul Henderson, Hakan Bilen, Niloy J Mitra, and Paul Guerrero. Renderdiffusion: Image diffusion for 3d reconstruction, inpainting and generation. In *Proceedings of the IEEE/CVF Conference on Computer Vision and Pattern Recognition*, pages 12608–12618, 2023. 1, 2
- [3] Minwoo Byeon, Beomhee Park, Haecheon Kim, Sungjun Lee, Woonhyuk Baek, and Saehoon Kim. Coyo-700m: Image-text pair dataset. <https://github.com/kakaobrain/coyo-dataset>, 2022. 1
- [4] Eric R Chan, Connor Z Lin, Matthew A Chan, Koki Nagano, Boxiao Pan, Shalini De Mello, Orazio Gallo, Leonidas J Guibas, Jonathan Tremblay, Sameh Khamis, et al. Efficient geometry-aware 3d generative adversarial networks. In *Proceedings of the IEEE/CVF Conference on Computer Vision and Pattern Recognition*, pages 16123–16133, 2022. 2
- [5] Eric R. Chan, Koki Nagano, Matthew A. Chan, Alexander W. Bergman, Jeong Joon Park, Axel Levy, Miika Aittala, Shalini De Mello, Tero Karras, and Gordon Wetzstein. GeNVS: Generative novel view synthesis with 3D-aware diffusion models. In *arXiv*, 2023. 1, 2
- [6] Angel X Chang, Thomas Funkhouser, Leonidas Guibas, Pat Hanrahan, Qixing Huang, Zimo Li, Silvio Savarese, Manolis Savva, Shuran Song, Hao Su, et al. Shapenet: An information-rich 3d model repository. *arXiv preprint arXiv:1512.03012*, 2015. 1, 2
- [7] Rui Chen, Yongwei Chen, Ningxin Jiao, and Kui Jia. Fantasia3d: Disentangling geometry and appearance for high-quality text-to-3d content creation. *arXiv preprint arXiv:2303.13873*, 2023. 2
- [8] Yen-Chi Cheng, Hsin-Ying Lee, Sergey Tulyakov, Alexander G Schwing, and Liang-Yan Gui. Sdfusion: Multimodal 3d shape completion, reconstruction, and generation. In *Proceedings of the IEEE/CVF Conference on Computer Vision and Pattern Recognition*, pages 4456–4465, 2023. 2
- [9] Matt Deitke, Ruoshi Liu, Matthew Wallingford, Huong Ngo, Oscar Michel, Aditya Kusupati, Alan Fan, Christian Laforte, Vikram Voleti, Samir Yitzhak Gadre, et al. Objaverse-xl: A universe of 10m+ 3d objects. *arXiv preprint arXiv:2307.05663*, 2023. 2, 5

- [10] Matt Deitke, Dustin Schwenk, Jordi Salvador, Luca Weihs, Oscar Michel, Eli VanderBilt, Ludwig Schmidt, Kiana Ehsani, Aniruddha Kembhavi, and Ali Farhadi. Objaverse: A universe of annotated 3d objects. In *Proceedings of the IEEE/CVF Conference on Computer Vision and Pattern Recognition*, pages 13142–13153, 2023. [1](#), [2](#), [5](#), [8](#), [13](#), [14](#)
- [11] Prafulla Dhariwal and Alexander Nichol. Diffusion models beat gans on image synthesis. *Advances in neural information processing systems*, 34:8780–8794, 2021. [3](#)
- [12] Leo Dorst, Daniel Fontijne, and Stephen Mann. *Geometric algebra for computer science: an object-oriented approach to geometry*. Elsevier, 2010. [4](#)
- [13] Laura Downs, Anthony Francis, Nate Koenig, Brandon Kinman, Ryan Hickman, Krista Reymann, Thomas B McHugh, and Vincent Vanhoucke. Google scanned objects: A high-quality dataset of 3d scanned household items. In *2022 International Conference on Robotics and Automation (ICRA)*, pages 2553–2560. IEEE, 2022. [5](#), [13](#), [14](#)
- [14] Ziya Erkoç, Fangchang Ma, Qi Shan, Matthias Nießner, and Angela Dai. Hyperdiffusion: Generating implicit neural fields with weight-space diffusion. *arXiv preprint arXiv:2303.17015*, 2023. [2](#)
- [15] Patrick Esser, Robin Rombach, and Bjorn Ommer. Taming transformers for high-resolution image synthesis. In *Proceedings of the IEEE/CVF Conference on Computer Vision and Pattern Recognition*, pages 12873–12883, 2021. [3](#)
- [16] Jun Gao, Tianchang Shen, Zian Wang, Wenzheng Chen, Kangxue Yin, Daiqing Li, Or Litany, Zan Gojcic, and Sanja Fidler. Get3d: A generative model of high quality 3d textured shapes learned from images. In *Advances In Neural Information Processing Systems*, 2022. [2](#)
- [17] Jiatao Gu, Alex Trevithick, Kai-En Lin, Josh Susskind, Christian Theobalt, Lingjie Liu, and Ravi Ramamoorthi. Nerfdiff: Single-image view synthesis with nerf-guided distillation from 3d-aware diffusion. In *International Conference on Machine Learning*, 2023. [1](#), [2](#)
- [18] Yuan-Chen Guo, Ying-Tian Liu, Ruizhi Shao, Christian Laforte, Vikram Voleti, Guan Luo, Chia-Hao Chen, Zi-Xin Zou, Chen Wang, Yan-Pei Cao, and Song-Hai Zhang. threestudio: A unified framework for 3d content generation. <https://github.com/threestudio-project/threestudio>, 2023. [5](#)
- [19] Jonathan Ho and Tim Salimans. Classifier-free diffusion guidance. *arXiv preprint arXiv:2207.12598*, 2022. [13](#)
- [20] Jonathan Ho, Ajay Jain, and Pieter Abbeel. Denoising diffusion probabilistic models. *arXiv preprint arXiv:2006.11239*, 2020. [1](#), [2](#), [3](#)
- [21] Edward J Hu, Phillip Wallis, Zeyuan Allen-Zhu, Yuanzhi Li, Shean Wang, Lu Wang, Weizhu Chen, et al. Lora: Low-rank adaptation of large language models. In *International Conference on Learning Representations*, 2021. [2](#)
- [22] Andrew Jaegle, Felix Gimeno, Andy Brock, Oriol Vinyals, Andrew Zisserman, and Joao Carreira. Perceiver: General perception with iterative attention. In *International conference on machine learning*, pages 4651–4664. PMLR, 2021. [4](#)
- [23] Heewoo Jun and Alex Nichol. Shap-e: Generating conditional 3d implicit functions. *arXiv preprint arXiv:2305.02463*, 2023. [2](#)
- [24] Animesh Karnewar, Andrea Vedaldi, David Novotny, and Niloy J Mitra. Holodiffusion: Training a 3d diffusion model using 2d images. In *Proceedings of the IEEE/CVF Conference on Computer Vision and Pattern Recognition*, pages 18423–18433, 2023. [2](#)
- [25] Tero Karras, Miika Aittala, Timo Aila, and Samuli Laine. Elucidating the design space of diffusion-based generative models. *Advances in Neural Information Processing Systems*, 35:26565–26577, 2022. [1](#), [2](#)
- [26] Chiheon Kim, Doyup Lee, Saehoon Kim, Minsu Cho, and Wook-Shin Han. Generalizable implicit neural representations via instance pattern composers. In *Proceedings of the IEEE/CVF Conference on Computer Vision and Pattern Recognition*, pages 11808–11817, 2023. [9](#)
- [27] Lambda Labs. Stable diffusion image variations model card. <https://huggingface.co/lambdalabs/stable-diffusion-image-conditioned>, 2022. [2](#)
- [28] Doyup Lee, Chiheon Kim, Minsu Cho, and Wook-Shin Han. Locality-aware generalizable implicit neural representation. In *Thirty-seventh Conference on Neural Information Processing Systems*, 2023. [9](#)
- [29] Yuheng Li, Haotian Liu, Qingyang Wu, Fangzhou Mu, Jianwei Yang, Jianfeng Gao, Chunyuan Li, and Yong Jae Lee. Gligen: Open-set grounded text-to-image generation. In *Proceedings of the IEEE/CVF Conference on Computer Vision and Pattern Recognition*, pages 22511–22521, 2023. [2](#)
- [30] Chen-Hsuan Lin, Jun Gao, Luming Tang, Towaki Takikawa, Xiaohui Zeng, Xun Huang, Karsten Kreis, Sanja Fidler, Ming-Yu Liu, and Tsung-Yi Lin. Magic3d: High-resolution text-to-3d content creation. In *Proceedings of the IEEE/CVF Conference on Computer Vision and Pattern Recognition*, pages 300–309, 2023. [2](#), [5](#)
- [31] Minghua Liu, Ruoxi Shi, Linghao Chen, Zhuoyang Zhang, Chao Xu, Hansheng Chen, Chong Zeng, Jiayuan Gu, and Hao Su. One-2-3-45++: Fast single image to 3d objects with consistent multi-view generation and 3d diffusion, 2023. [1](#), [2](#), [9](#)
- [32] Ruoshi Liu, Rundi Wu, Basile Van Hoorick, Pavel Tokmakov, Sergey Zakharov, and Carl Vondrick. Zero-1-to-3: Zero-shot one image to 3d object. *arXiv preprint arXiv:2303.11328*, 2023. [2](#), [4](#), [5](#), [13](#)
- [33] Yuan Liu, Cheng Lin, Zijiao Zeng, Xiaoxiao Long, Lingjie Liu, Taku Komura, and Wenping Wang. Syncdreamer: Generating multiview-consistent images from a single-view image. *arXiv preprint arXiv:2309.03453*, 2023. [2](#), [6](#), [13](#)
- [34] Xiaoxiao Long, Yuan-Chen Guo, Cheng Lin, Yuan Liu, Zhiyang Dou, Lingjie Liu, Yuexin Ma, Song-Hai Zhang, Marc Habermann, Christian Theobalt, et al. Wonder3d: Single image to 3d using cross-domain diffusion. *arXiv preprint arXiv:2310.15008*, 2023. [1](#), [2](#)
- [35] Luke Melas-Kyriazi, Iro Laina, Christian Rupprecht, and Andrea Vedaldi. Realfusion: 360deg reconstruction of any object from a single image. In *Proceedings of the IEEE/CVF Conference on Computer Vision and Pattern Recognition*, pages 8446–8455, 2023. [2](#)

- [36] Ben Mildenhall, Pratul P Srinivasan, Matthew Tancik, Jonathan T Barron, Ravi Ramamoorthi, and Ren Ng. Nerf: Representing scenes as neural radiance fields for view synthesis. *Communications of the ACM*, 65(1):99–106, 2021. [1](#), [4](#)
- [37] Chong Mou, Xintao Wang, Liangbin Xie, Yanze Wu, Jian Zhang, Zhongang Qi, Ying Shan, and Xiaohu Qie. T2i-adapter: Learning adapters to dig out more controllable ability for text-to-image diffusion models. *arXiv preprint arXiv:2302.08453*, 2023. [2](#)
- [38] Norman Müller, Yawar Siddiqui, Lorenzo Porzi, Samuel Rota Buló, Peter Kotschieder, and Matthias Nießner. Diffri: Rendering-guided 3d radiance field diffusion. In *Proceedings of the IEEE/CVF Conference on Computer Vision and Pattern Recognition*, pages 4328–4338, 2023. [2](#)
- [39] Thomas Müller, Alex Evans, Christoph Schied, and Alexander Keller. Instant neural graphics primitives with a multi-resolution hash encoding. *ACM Transactions on Graphics (ToG)*, 41(4):1–15, 2022. [1](#), [2](#), [5](#)
- [40] Gimin Nam, Mariem Khlifi, Andrew Rodriguez, Alberto Tono, Linqi Zhou, and Paul Guerrero. 3d-ldm: Neural implicit 3d shape generation with latent diffusion models. *arXiv preprint arXiv:2212.00842*, 2022. [2](#)
- [41] Alex Nichol, Heewoo Jun, Pratul Dhariwal, Pamela Mishkin, and Mark Chen. Point-e: A system for generating 3d point clouds from complex prompts. *arXiv preprint arXiv:2212.08751*, 2022. [2](#)
- [42] Michael Niemeyer and Andreas Geiger. Giraffe: Representing scenes as compositional generative neural feature fields. In *Proc. IEEE Conf. on Computer Vision and Pattern Recognition (CVPR)*, 2021. [2](#)
- [43] Evangelos Ntavelis, Aliaksandr Siarohin, Kyle Olszewski, Chaoyang Wang, Luc Van Gool, and Sergey Tulyakov. Autodecoding latent 3d diffusion models. *arXiv preprint arXiv:2307.05445*, 2023. [2](#)
- [44] Ben Poole, Ajay Jain, Jonathan T Barron, and Ben Mildenhall. Dreamfusion: Text-to-3d using 2d diffusion. In *The Eleventh International Conference on Learning Representations*, 2022. [2](#), [5](#), [6](#), [14](#)
- [45] Alec Radford, Jong Wook Kim, Chris Hallacy, Aditya Ramesh, Gabriel Goh, Sandhini Agarwal, Girish Sastry, Amanda Askell, Pamela Mishkin, Jack Clark, Gretchen Krueger, and Ilya Sutskever. Learning transferable visual models from natural language supervision. In *Proceedings of the 38th International Conference on Machine Learning*, pages 8748–8763. PMLR, 2021. [5](#)
- [46] René Ranftl, Alexey Bochkovskiy, and Vladlen Koltun. Vision transformers for dense prediction. In *Proceedings of the IEEE/CVF international conference on computer vision*, pages 12179–12188, 2021. [8](#)
- [47] Jeremy Reizenstein, Roman Shapovalov, Philipp Henzler, Luca Sbordone, Patrick Labatut, and David Novotny. Common objects in 3d: Large-scale learning and evaluation of real-life 3d category reconstruction. In *Proceedings of the IEEE/CVF International Conference on Computer Vision*, pages 10901–10911, 2021. [1](#), [2](#)
- [48] Robin Rombach, Andreas Blattmann, Dominik Lorenz, Patrick Esser, and Björn Ommer. High-resolution image synthesis with latent diffusion models. In *Proceedings of the IEEE/CVF conference on computer vision and pattern recognition*, pages 10684–10695, 2022. [1](#), [3](#), [8](#)
- [49] Olaf Ronneberger, Philipp Fischer, and Thomas Brox. U-net: Convolutional networks for biomedical image segmentation. In *Medical Image Computing and Computer-Assisted Intervention—MICCAI 2015: 18th International Conference, Munich, Germany, October 5-9, 2015, Proceedings, Part III 18*, pages 234–241. Springer, 2015. [3](#)
- [50] Christoph Schuhmann, Romain Beaumont, Richard Vencu, Cade Gordon, Ross Wightman, Mehdi Cherti, Theo Coombes, Aarush Katta, Clayton Mullis, Mitchell Wortsman, et al. Laion-5b: An open large-scale dataset for training next generation image-text models. *Advances in Neural Information Processing Systems*, 35:25278–25294, 2022. [1](#)
- [51] Junyoung Seo, Wooseok Jang, Min-Seop Kwak, Jaehoon Ko, Hyeonsu Kim, Junho Kim, Jin-Hwa Kim, Jiyoung Lee, and Seungryong Kim. Let 2d diffusion model know 3d-consistency for robust text-to-3d generation. *arXiv preprint arXiv:2303.07937*, 2023. [2](#)
- [52] Tianchang Shen, Jun Gao, Kangxue Yin, Ming-Yu Liu, and Sanja Fidler. Deep marching tetrahedra: a hybrid representation for high-resolution 3d shape synthesis. *Advances in Neural Information Processing Systems*, 34:6087–6101, 2021. [2](#)
- [53] Jing Shi, Wei Xiong, Zhe Lin, and Hyun Joon Jung. Instant-booth: Personalized text-to-image generation without test-time finetuning. *arXiv preprint arXiv:2304.03411*, 2023. [5](#)
- [54] Ruoxi Shi, Hansheng Chen, Zhuoyang Zhang, Minghua Liu, Chao Xu, Xinyue Wei, Linghao Chen, Chong Zeng, and Hao Su. Zero123++: a single image to consistent multi-view diffusion base model. *arXiv preprint arXiv:2310.15110*, 2023. [1](#), [2](#), [8](#), [13](#)
- [55] Yichun Shi, Peng Wang, Jianglong Ye, Mai Long, Kejie Li, and Xiao Yang. Mvdream: Multi-view diffusion for 3d generation. *arXiv preprint arXiv:2308.16512*, 2023. [1](#), [2](#)
- [56] J Ryan Shue, Eric Ryan Chan, Ryan Po, Zachary Ankner, Jiajun Wu, and Gordon Wetzstein. 3d neural field generation using triplane diffusion. In *Proceedings of the IEEE/CVF Conference on Computer Vision and Pattern Recognition*, pages 20875–20886, 2023. [2](#)
- [57] Yang Song and Stefano Ermon. Generative modeling by estimating gradients of the data distribution. *Advances in neural information processing systems*, 32, 2019. [1](#), [2](#)
- [58] Hossein Talebi and Peyman Milanfar. Learned perceptual image enhancement. In *2018 IEEE international conference on computational photography (ICCP)*, pages 1–13. IEEE, 2018. [5](#)
- [59] Ashish Vaswani, Noam Shazeer, Niki Parmar, Jakob Uszkoreit, Llion Jones, Aidan N Gomez, Łukasz Kaiser, and Illia Polosukhin. Attention is all you need. In *Advances in neural information processing systems*, pages 5998–6008, 2017. [4](#)
- [60] Haochen Wang, Xiaodan Du, Jiahao Li, Raymond A Yeh, and Greg Shakhnarovich. Score jacobian chaining: Lifting pretrained 2d diffusion models for 3d generation. In *Pro-*

- ceedings of the IEEE/CVF Conference on Computer Vision and Pattern Recognition*, pages 12619–12629, 2023. 2
- [61] Peng Wang, Lingjie Liu, Yuan Liu, Christian Theobalt, Taku Komura, and Wenping Wang. Neus: Learning neural implicit surfaces by volume rendering for multi-view reconstruction. *Advances in Neural Information Processing Systems*, 34:27171–27183, 2021. 2
- [62] Yiming Wang, Qin Han, Marc Habermann, Kostas Daniilidis, Christian Theobalt, and Lingjie Liu. Neus2: Fast learning of neural implicit surfaces for multi-view reconstruction. *arXiv preprint arXiv:2212.05231*, 2022. 2
- [63] Zhengyi Wang, Cheng Lu, Yikai Wang, Fan Bao, Chongxuan Li, Hang Su, and Jun Zhu. Prolificdreamer: High-fidelity and diverse text-to-3d generation with variational score distillation. *arXiv preprint arXiv:2305.16213*, 2023. 2
- [64] Daniel Watson, William Chan, Ricardo Martin Brullalla, Jonathan Ho, Andrea Tagliasacchi, and Mohammad Norouzi. Novel view synthesis with diffusion models. In *The Eleventh International Conference on Learning Representations*, 2023. 1, 2, 4
- [65] Yang Xue, Yuheng Li, Krishna Kumar Singh, and Yong Jae Lee. Giraffe hd: A high-resolution 3d-aware generative model. In *Proceedings of the IEEE/CVF Conference on Computer Vision and Pattern Recognition*, pages 18440–18449, 2022. 2
- [66] Jiayu Yang, Ziang Cheng, Yunfei Duan, Pan Ji, and Hongdong Li. Consistnet: Enforcing 3d consistency for multi-view images diffusion. *arXiv preprint arXiv:2310.10343*, 2023. 2
- [67] Alex Yu, Vickie Ye, Matthew Tancik, and Angjoo Kanazawa. pixelnerf: Neural radiance fields from one or few images. In *Proceedings of the IEEE/CVF Conference on Computer Vision and Pattern Recognition*, pages 4578–4587, 2021. 2
- [68] Xianggang Yu, Mutian Xu, Yidan Zhang, Haolin Liu, Chongjie Ye, Yushuang Wu, Zizheng Yan, Chenming Zhu, Zhangyang Xiong, Tianyou Liang, et al. Mvimnet: A large-scale dataset of multi-view images. In *Proceedings of the IEEE/CVF Conference on Computer Vision and Pattern Recognition*, pages 9150–9161, 2023. 1, 2
- [69] Xiaohui Zeng, Arash Vahdat, Francis Williams, Zan Gojcic, Or Litany, Sanja Fidler, and Karsten Kreis. Lion: Latent point diffusion models for 3d shape generation. In *Advances in Neural Information Processing Systems (NeurIPS)*, 2022. 2
- [70] Lyumin Zhang. Reference-only control. <https://github.com/Mikubill/sd-webui-controlnet/discussions/1236>, 2023. 2
- [71] Lvmin Zhang and Maneesh Agrawala. Adding conditional control to text-to-image diffusion models. *arXiv preprint arXiv:2302.05543*, 2023. 2, 8, 14
- [72] Zhizhuo Zhou and Shubham Tulsiani. Sparsefusion: Distilling view-conditioned diffusion for 3d reconstruction. In *Proceedings of the IEEE/CVF Conference on Computer Vision and Pattern Recognition*, pages 12588–12597, 2023. 1, 2

A. Implementation Details

We describe the implementation details of our NVS-Adapter for reproducibility. We have implemented our NVS-Adapter using the framework of Stable Diffusion 2.1-base [1]. We add the cross-attentions of our NVS-Adapter, where each cross-attention has the same dimensionality as the text cross-attention of each U-Net block. We add the NVS-Adapter modules into every U-Net block of Stable Diffusion. Our NVS-Adapter predicts $N = 4$ target views at once from a single reference image. The target views alignment uses $h \times w$ learnable tokens at every U-Net block, where $h \times w$ is equal to the resolution of each U-Net feature map. We train our NVS-Adapter on Objaverse [10], which includes 800K 3D assets, and adopt the same training data of rendered views with 256 resolution as Zero-1-to-3 [32]. Our model is trained for 200K iterations with 256 total batch size using 16 NVIDIA A100 80GB GPUs for 5 days, while ablation studies are conducted on the checkpoints at 100K iterations due to the limited computational resources. A linear warmup of learning rate is used during the first 10K iterations, where the peak learning rate is 0.00005. We use an exponential moving average (EMA) of trainable parameters with 0.9995 decay rate. Note that the parameters of Stable Diffusion are not updated during training. We randomly drop the information of reference images for 10% of training samples to apply classifier-free guidance (CFG) [19] during view generation. To drop the information of reference images, we replace the global semantic conditioning and positional embeddings with zero embeddings, and replace the U-Net input of reference images with Gaussian noises. We use 11.0 scale of CFG during inference. The codes and evaluation samples will be released to ensure the reproducibility of our results.

B. Generalizing the Number of Target Views

We evaluate the changes of the number of target views, considering that our NVS-Adapter is flexible to generalize the number of target views. Specifically, after a framework with NVS-Adapter is trained to synthesize $N_{\text{train}} = \{1, 2, 4, 6\}$ target views, $N_{\text{eval}} = \{1, 2, 4, 6, 16\}$ target views are generated at once during inference. Table A shows PSNR, SSIM, and LPIPS scores on GSO [13] according to different pairs of $(N_{\text{train}}, N_{\text{eval}})$. When our framework with NVS-Adapter is trained to synthesize a single target view as $N_{\text{train}} = 1$, the results are competitive with other settings. However, the framework with $N_{\text{train}} = 1$ fails to synthesize multiple views at once and cannot generalize to increase the number of target views for consistent novel view synthesis. However, when our frameworks with $N_{\text{train}} = \{2, 4, 6\}$ are trained to synthesize multiple views at once, our frameworks can increase the number of target views. The NVS-Adapter with $N_{\text{train}=4}$ shows well-balanced results on various number of target views, while achieving its best performance on $N_{\text{eval}} = 16$. Thus, we have finally selected $N_{\text{train}} = 4$ as our main hyper-parameter setup, considering its generalization capability.

Table A. The effects of the number of target views N on GSO. The first four rows report PSNR scores, the next four rows report SSIM, and the last four rows report LPIPS, with varying the number of target views for training and evaluation.

		$N_{\text{eval}} = 1$	$N_{\text{eval}} = 2$	$N_{\text{eval}} = 4$	$N_{\text{eval}} = 6$	$N_{\text{eval}} = 16$
PSNR	$N_{\text{train}} = 1$	18.45	15.09	14.58	14.50	14.38
	$N_{\text{train}} = 2$	18.42	18.70	18.62	18.67	18.55
	$N_{\text{train}} = 4$	17.08	18.01	18.56	18.67	19.01
	$N_{\text{train}} = 6$	15.09	16.23	17.44	17.85	18.38
SSIM	$N_{\text{train}} = 1$	0.8409	0.8057	0.8013	0.8013	0.8025
	$N_{\text{train}} = 2$	0.8427	0.8453	0.8450	0.8453	0.8451
	$N_{\text{train}} = 4$	0.8237	0.8374	0.8446	0.8456	0.8501
	$N_{\text{train}} = 6$	0.7924	0.8126	0.8288	0.8333	0.8419
LPIPS	$N_{\text{train}} = 1$	0.1240	0.1706	0.1800	0.1805	0.1812
	$N_{\text{train}} = 2$	0.1239	0.1215	0.1219	0.1217	0.1221
	$N_{\text{train}} = 4$	0.1460	0.1307	0.1243	0.1228	0.1190
	$N_{\text{train}} = 6$	0.1796	0.1581	0.1397	0.1335	0.1254

C. Comparisons of NVS-Adapter with Concurrent Work

We compare the qualitative results of our NVS-Adapter with our concurrent projects such as SyncDreamer [33] and Zero123++ [54], which synthesize multiple novel views at once. Note that SyncDreamer and Zero123++ can only synthesize the novel views under predefined and fixed camera poses, while finetuning the whole parameters of T2I models. However, our NVS-Adapter is more flexible than SyncDreamer and Zero123++, since our framework can synthesize novel



Figure A. Novel view synthesis examples by SyncDreamer and our NVS-Adapter.

views under arbitrary camera poses. Despite an unfair comparison, we synthesize the novel views of GSO under the predefined camera poses of SyncDreamer and Zero123++. Figure A, Figure B represent the synthesized novel views to compare our NVS-Adapter with SyncDreamer and Zero123++ respectively. Although our NVS-Adapter preserves the original parameters of T2I models, our frameworks synthesize geometrically consistent multi-views, demonstrating competitive results with SyncDreamer and Zero123++.

D. More Qualitative Results

We attach more qualitative results in the main paper. Figure C shows the results generated by our NVS-Adapter with and without global semantic conditioning(GSC). We found in many cases, NVS-Adapter fails to capture global semantics without GSC. Figure D shows the additional results of generated views when our NVS-Adapter is combined with ControlNet [71] or not. Figure E and Figure F show the examples of generated novel views on Objaverse [10] and GSO [13], respectively. Figure G shows the results of generated views from arbitrary reference images, which are collected on the internet. Figure H and Figure I show the examples of text to multi-views, where the reference images are generated by the T2I model. Figure J and Figure K show additional results on score distillation sampling(SDS) [44] to generate 3D objects. We also attach videos for the generated 3D. Figure L visualizes attention maps of target view alignments, which aggregate the information of target views into learnable tokens.

E. Failure Cases

Figure M shows the failure cases of our model. The first example shows the case where NVS-Adapter misunderstands the direction of cars although the rider (bart) is reliably rendered. The second example assumes the object to be a thin-plane object. Since Objaverse includes numerous thin-plane objects, the model can result in volumeless generation. In the case of the third example, the doll has inconsistent color for the unobserved parts in a reference image. Although unobserved parts are ambiguous, the synthesized colors do not make sense in general. Indeed, the color of the back should be purple rather than yellow. The last example seems strange since the ghost is located above the dish, indicating wrong topology between the ghost and the dish. We believe that increasing the scale of the training dataset can improve the performance of our NVS-Adapter.

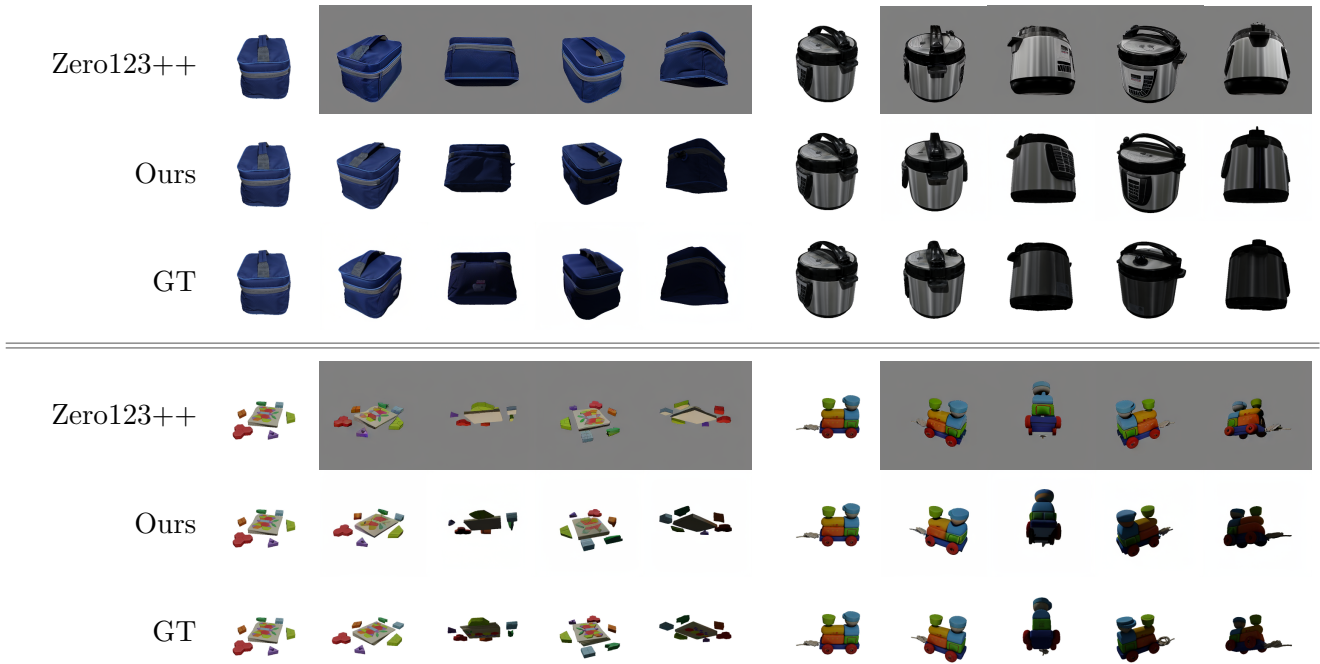


Figure B. Novel view synthesis examples by Zero123++ and our NVS-Adapter.

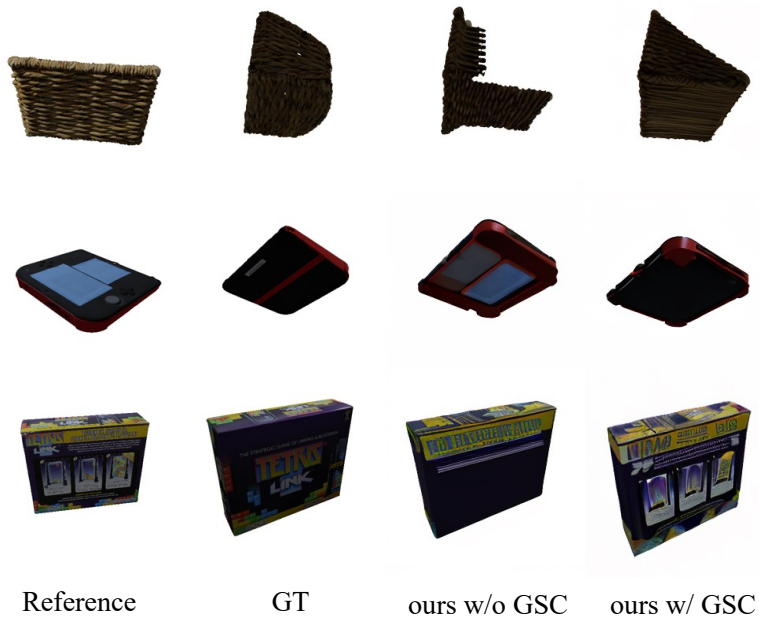


Figure C. Novel view synthesis examples by our NVS-Adapter with and without global semantic conditioning(GSC). Our NVS-Adapter without GSC often fails to capture global semantics from a reference view.

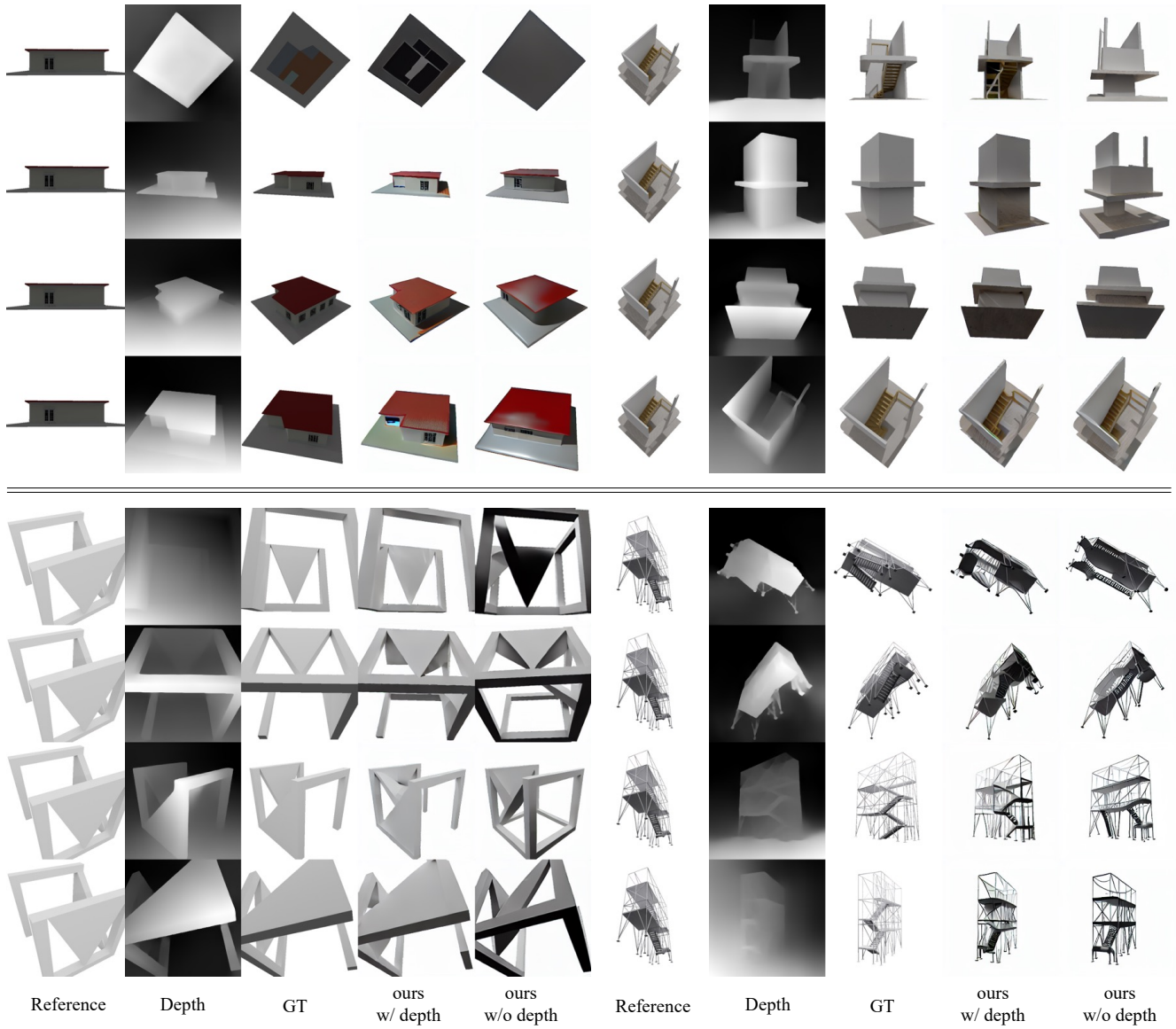


Figure D. Examples of novel view synthesis using our NVS-Adapter with and without depth conditions.

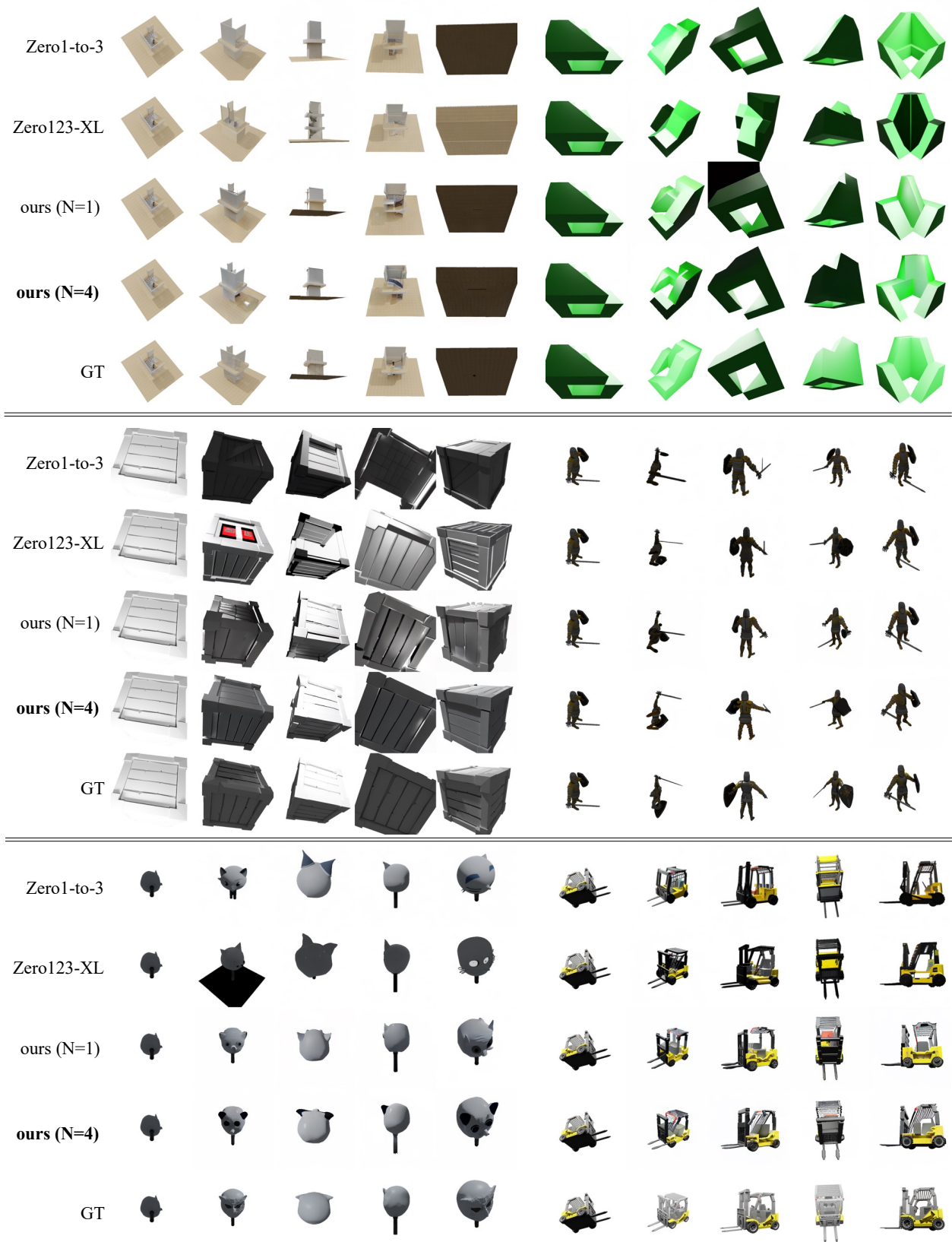


Figure E. Novel view synthesis examples by Zero-1-to-3, Zero123-XL, and our NVS-Adapter with $N = 1$ and $N = 4$ on Objaverse.

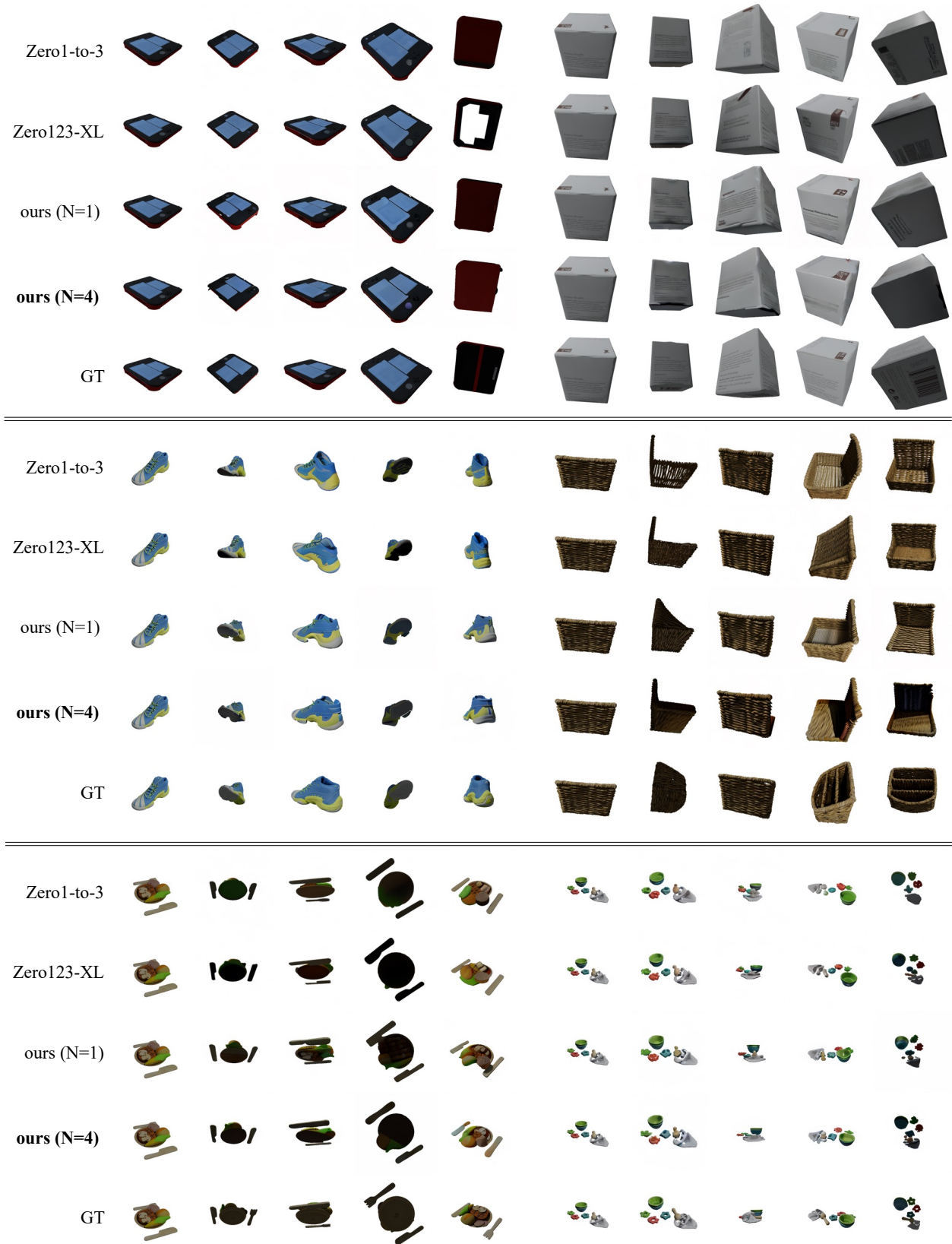


Figure F. Novel view synthesis examples by Zero-1-to-3, Zero123-XL, and our NVS-Adapter with $N = 1$ and $N = 4$ on GSO.

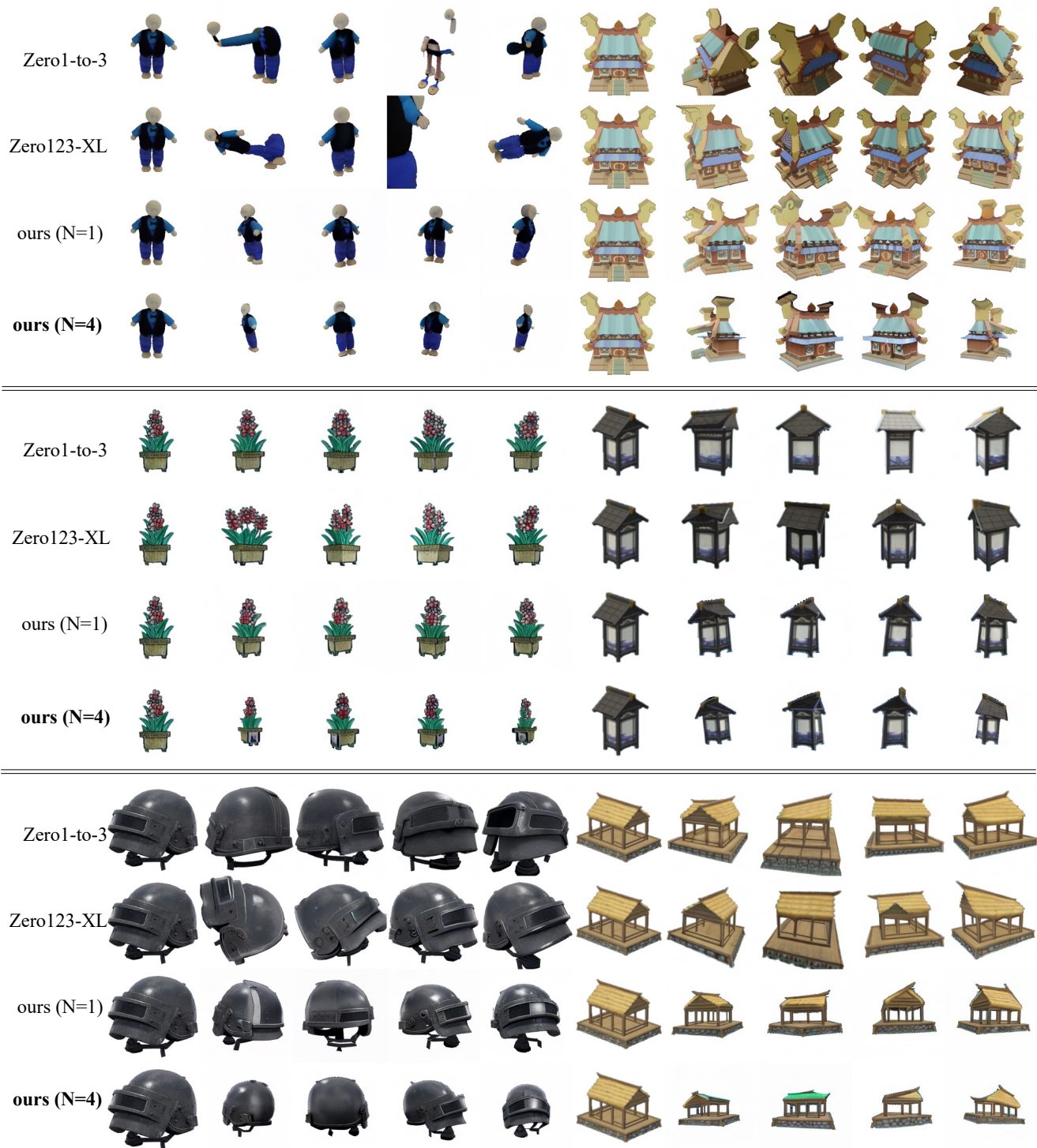


Figure G. Novel view synthesis examples by Zero-1-to-3, Zero123-XL, and our NVS-Adapter with $N = 1$ and $N = 4$ on reference images from the internet.

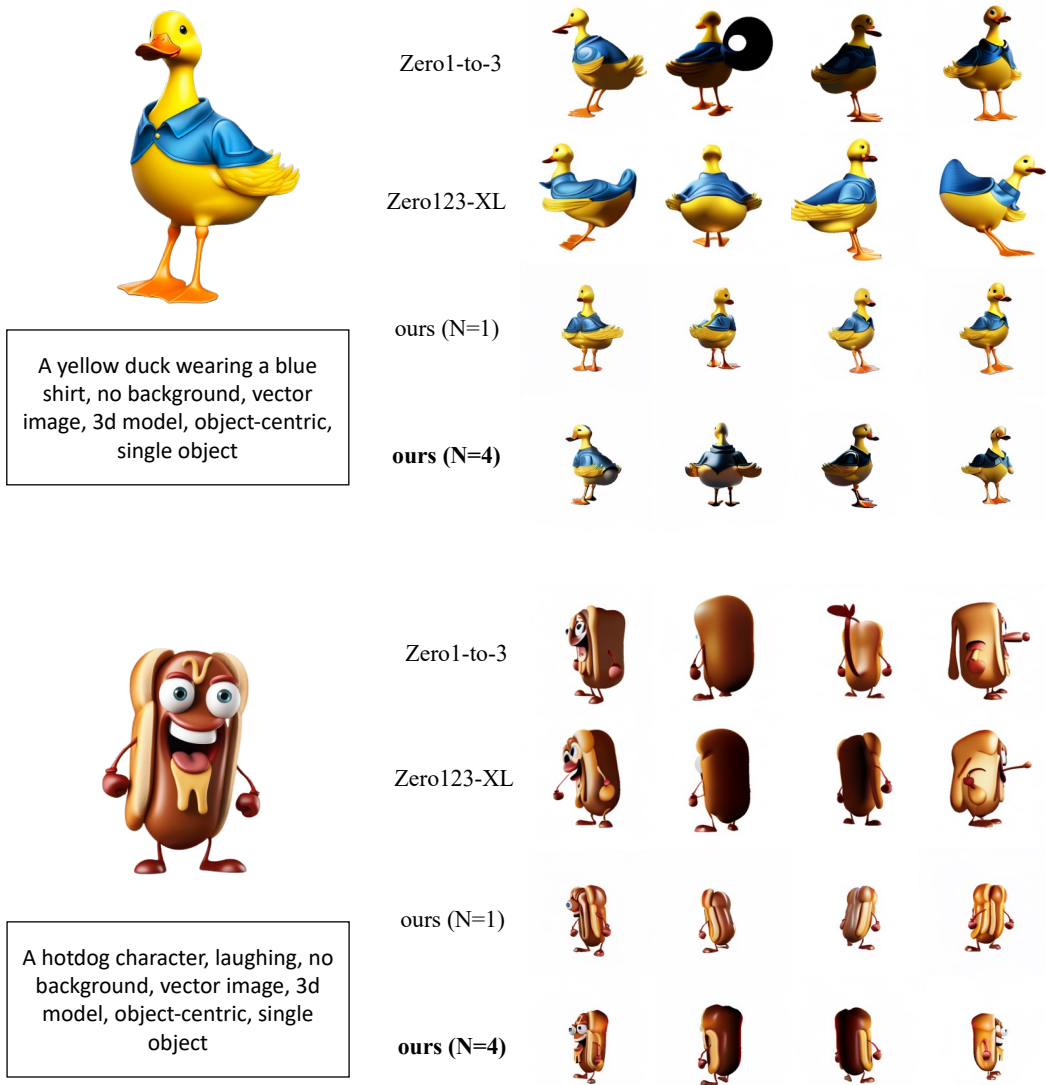


Figure H. Novel view synthesis examples by Zero-1-to-3, Zero123-XL, and our NVS-Adapter with $N = 1$ and $N = 4$ on images generated from text prompts.

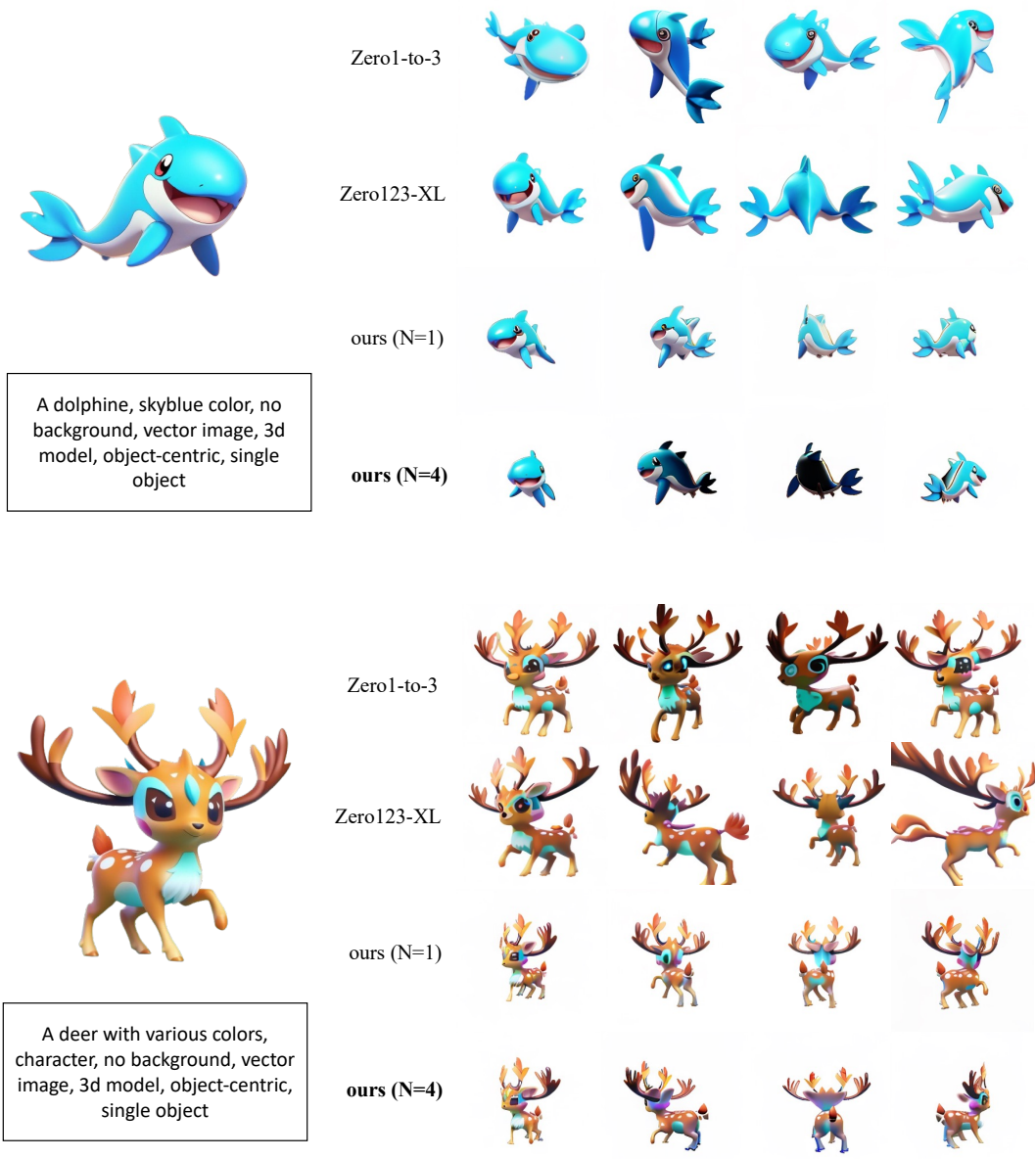


Figure I. Novel view synthesis examples by Zero-1-to-3, Zero123-XL, and our NVS-Adapter with $N = 1$ and $N = 4$ on images generated from text prompts.

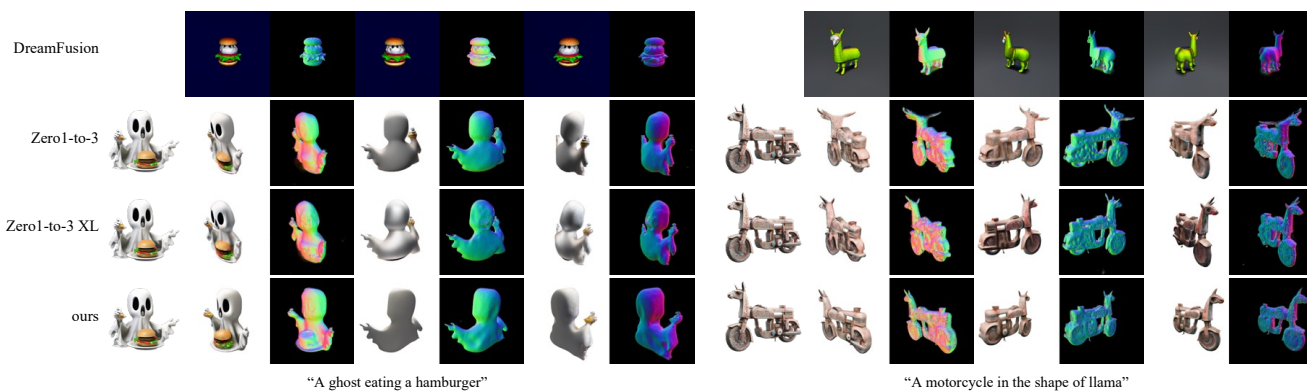
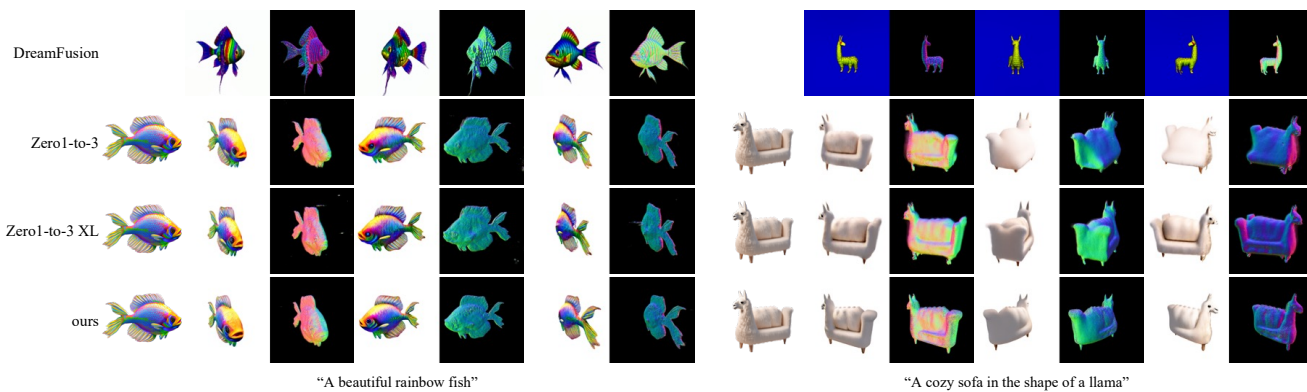


Figure J. 3D reconstruction examples via Score Distillation Sampling (SDS) with baselines and our NVS-Adapter. Images shows 3D reconstructions results conditioned on an image generated by T2I model.



Figure K. 3D reconstruction examples via Score Distillation Sampling (SDS) with baselines and our NVS-Adapter. Images shows 3D reconstructions results on an image from the internet.

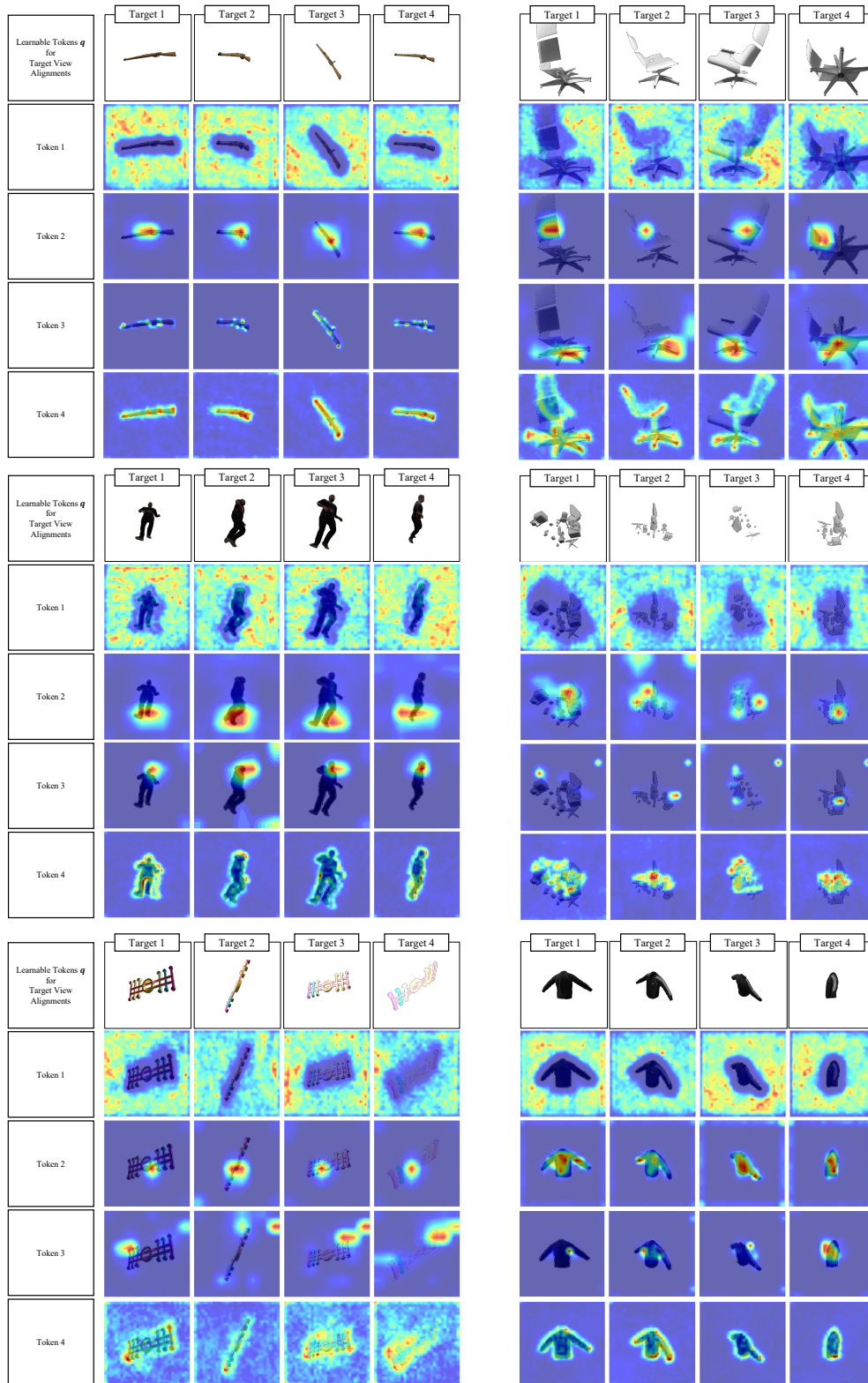


Figure L. Visualization of attention maps of target views alignment. Each token aggregates different regions of target views.

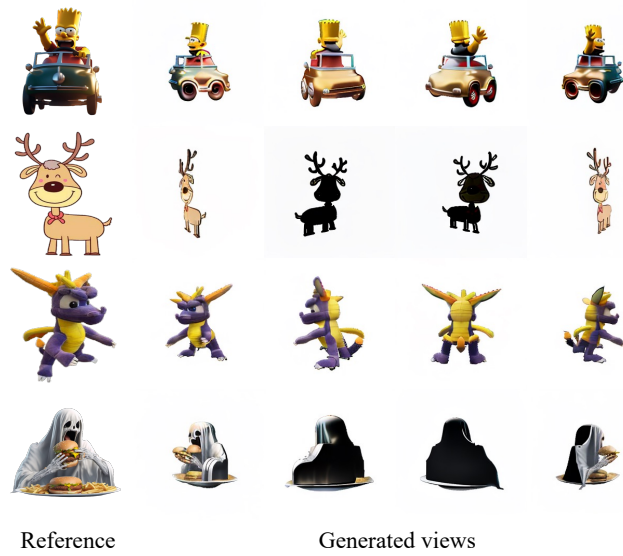


Figure M. Several failure cases of our NVS-Adapter. The first column shows reference images and the rest of the columns are rendered novel views.